8-22-2019

Dimension-breaking for Traveling Waves in Interfacial Flows

Matthew W. Seiders

DIMENSION-BREAKING FOR TRAVELING WAVES IN INTERFACIAL FLOWS

DISSERTATION

Matthew W. Seiders, Maj, USAF

AFIT-ENC-DS-19-S-002

DEPARTMENT OF THE AIR FORCE
AIR UNIVERSITY

AIR FORCE INSTITUTE OF TECHNOLOGY

Wright-Patterson Air Force Base, Ohio

AFIT-ENC-DS-19-S-002

DIMENSION-BREAKING FOR TRAVELING WAVES IN INTERFACIAL FLOWS

DISSERTATION

Presented to the Faculty

Graduate School of Engineering and Management

Air Force Institute of Technology

Air University

Air Education and Training Command

in Partial Fulfillment of the Requirements for the

Degree of PhD in Applied Mathematics

Matthew W. Seiders, B.S., M.S.

Maj, USAF

August 22, 2019

AFIT-ENC-DS-19-S-002

DIMENSION-BREAKING FOR TRAVELING WAVES IN INTERFACIAL FLOWS

DISSERTATION

Matthew W. Seiders, B.S., M.S.
Maj, USAF

Committee Membership:

Dr. B. F. Akers
Chair

Dr. A. W. Wood
Member

Capt R. P. Uber, PhD
Member

Maj J. A. Hess, PhD
Member

To my wife

as we continue our journey together

Acknowledgements

I sincerely appreciate the support and guidance provided by my research advisor, Dr. Benjamin Akers. His infinite patience has enabled me to succeed.

Matthew W. Seiders

Abstract

Fluid flow models in two spatial dimensions with a one-dimensional interface are known to support overturned traveling solutions. Computational methods of solving the two-dimensional problem are well developed [1, 2], even in the case of overturned waves. The three-dimensional problem is harder for three prominent reasons. First, some formulations of the two-dimensional problem do not extend to three-dimensions. The technique of conformal mapping is a prime example, as it is very efficient in two dimensions but does not have a three-dimensional equivalent. Second, some three-dimensional models, such as the Transformed Field Expansion method [3], do not allow for overturned waves. Third, computational time can increase by more than an order of magnitude. For example, the Birkhoff-Rott integral has a cost of $O(N^2)$ in two-dimensions but $O(N^4M^2)$ in three-dimensions, where N is the number of discretized points in the lateral directions and M is the number of truncated summation terms.

This study seeks to bridge the gap between efficient two-dimensional numerical solvers and more computationally expensive three-dimensional solvers. The dissertation does so by developing a dimension-breaking continuation method, which is not limited to solving interfacial wave models. The method involves three steps: first, conduct N-dimensional continuation to large amplitude; second, extend the solution trivially to a (N+1)-dimensional solution and solve the linearization; and third, use the linearization to begin (N+1)-dimensional continuation. This method is successfully applied to Kadomtsev-Petviashvili and Akers-Milewski interfacial models and then in a reduced Vortex Sheet interfacial formulation. In doing so, accurate search directions are calculated for use in higher-dimension quasi-Newton solvers.

Table of Contents

Page

List of Figures

DIMENSION-BREAKING FOR TRAVELING WAVES IN INTERFACIAL FLOWS

I. Introduction

Equations in fluid mechanics are used to model many interesting physical systems. These include flows around rigid objects (e.g. water flowing past a pylon, or turbulent air flow past a wing or vehicle roof rack). Interfacial flows model the movement of two adjacent fluids, such as liquid/gas interfaces (e.g. the surface of a lake with ripples, trapped bubbles, or water droplets) and liquid/liquid interfaces (e.g. oil on the surface of water, or layers of ocean water of differing salinity). While this work is focused on one- and two-dimensional traveling interfacial waves, the concepts are not limited to fluid flows. The technique developed within this dissertation can be applied in any N-dimensional system at an equilibria point.

This work considers problems at the intersection of fluid mechanics and dynamical systems. In the fluid models studied, one-dimensional traveling wave interfaces are essentially fixed points of a dynamical system. The intention of this dissertation is to understand the bifurcation structure from these points in order to perform a newly proposed dimension-breaking numerical continuation method. This method will allow for an efficient increase in dimension, yielding accurate initial search directions for fully two-dimensional solvers. The proposed dimension-breaking method will do so by linearizing the one-dimensional model with a weakly-two-dimensional ansatz, then numerically solve the generalized eigenvalue problem arising from the linearization.

Computational methods are used to numerically solve mathematical models and equations. These methods are inherently faster at lower-dimension. For example,

fluid interface models of a two-dimensional wave require finding values of the surface over a grid of size N^2 (assuming N discretized points in both axes), whereas an interface model with a one-dimensional surface wave requires only N points.

Due to this cost reduction, lower-dimensional models are often used as an approximation for a higher-dimensional system, going so far as to use zero-dimensional (point) approximations of the system. A method to calculate the density of argon in a laser medium [5], and a study of the combustion and heat-release in an engine [6] are examples of lower-dimensional models being used for computational savings.

The computational efficiency gained in lower-dimensional models comes at the cost of losing information from the full system. This work proposes to instead gain efficiency by using a hybrid method. Instead of doing all computations in the higher-dimensional model, the proposed method uses a lower-dimensional model for a portion of the computation, then computes a search direction to effectively initialize a higher-dimensional model. This procedure requires a delicate understanding of the bifurcation from lower to higher dimensions.

1.1 History of Traveling Water Waves

The study of traveling water waves dates at least back to a report by J. Scott Russell to the British Association for the Advancement of Science in August 1834. He was observing a boat being towed rapidly through a canal when the vessel came to a sudden stop; a wave formed and began to traverse the canal at great speed, maintaining a steady shape. He followed the wave on horseback for a mile or two, before losing it to the turns of the canal [7]. His observations and subsequent experimental research are now credited as the discovery of non-linear solitary waves, though at the time it was not well understood [8].

G.G. Stokes followed with his 1847 paper "On the Theory of Oscillatory Waves",

giving accurate calculations for non-linear two-dimensional traveling waves [9]. While he advanced the field dramatically, he was not able to model Russell's solitary waves; a more robust understanding of non-linear solitary traveling waves would not come for almost 50 years [10]. In 1895, Korteweg and deVries showed that letting the period of the wave tend to infinity yielded a solitary wave solution in-line with Stokes' calculations and Russell's observation [11].

1.2 Current State of the Field

Two-dimensional fluid models (with a one-dimensional line interface between water and air) have been extensively studied over the last century. Some solutions of these various models, such as periodic Crapper waves and solitary Korteweg-deVries (KdV) waves, can be described with explicit formulas [12, 13].

The two-dimensional analogue of the KdV equation, the Kadomtsev-Petviashvili (KP) equation [14] has also been heavily researched. Tajiri and Murakami pursued a model of transversely periodic KP waves [15]. Groves, Haragus and Sun extended the work in [15] by providing existence proofs of transversely periodic waves in Euler's potential flow model. Solitary KdV waves that have been trivially extended to planar waves are an example of solutions in the KP model that undergo bifurcations to a family of transversely periodic KP waves [4].

In recent years, much work has been done on computational methods for various fluid models. Waves crashing onto a shore are an easy-to-visualize example of overturning waves in the time-dependent problem. With enough energy, water pushing up an inclined bottom will eventually overturn and break; it is not an uncommon phenomenon. Numerical simulations of a three-dimensional time-dependent Navier-Stokes model exist, though at a huge computational expense. They are in good agreement with observed wave experiments and include overturning, breaking, air

entrainment and spray formation [16].

In this study, we instead consider overturned traveling waves. These waves may occur as ripples moving away from a disturbance in a lake, or fuel flow in a channel where capillary forces dominate over the force of gravity [17].

Traveling wave solutions are interface profiles moving at a steady speed without changing shape in the reference frame; they are essentially stationary points of a dynamical system. Of current interest are steady, traveling waves with overturning features, of which Crapper and Meiron-Saffman waves [18, 19] are good examples. Over the last ten years, there has been much research into traveling waves, including their asymptotics, singularities and instabilities [20, 21, 22, 23, 24, 25].

To the best of the author's knowledge, there has only been one computational example of a fully three-dimensional overturned traveling wave at the time of this work [26]. That study used an ad-hoc dimension-breaking method in a vortex sheet formulation to find and compute the overturned wave. This dissertation seeks to continue in this area of research. By presenting formal asymptotics of the dimension-breaking bifurcation, the linearization is solved and three-dimensional waves are computed. A better understanding of the bifurcation structure associated with this and other models enables an efficient numerical method by providing a valid search direction for computing overturned traveling waves in a fully three-dimensional solver.

Applications of this work can extend to any two-dimensional equilibria with a corresponding three-dimensional extension. An example of a potential application area is a simulation to complement a recent study that has been conducted aboard the International Space Station of capillary channel flows [17], which exhibit overturned interfaces and are quasi-two-dimensional.

1.3 Governing Equations

This study uses three fluid flow interfacial models that are derived from Euler's equations. Some basics of these formulations are presented here and the models will be discussed in later sections.

Euler's Equations of Motion

The generally accepted equations for modeling the flow of an ideal fluid are Euler's equations, derived in a variety of texts such as Sir Horace Lamb's widely referenced *Hydrodynamics* [27] to more modern introductions such as Acheson's *Elementary Fluid Dynamics* [28]. An assumption that a fluid is ideal means that it is incompressible and of constant density, ρ.

In a three-dimensional domain in Cartesian coordinates, with x and y periodic horizontal components and z the vertical component, let $\mathbf{u}(x, y, z, t) = (u, v, w)$ be the velocity vector of an ideal fluid and $F(x, y, z, t)$ be the forces of pressure, p, and gravity, g, acting on a small volume, δV, of fluid. Then

$$F = (-\nabla p + \rho g)\delta V$$

The mass is the small volume, δV, of fluid multiplied by its density, ρ, and the acceleration of the fluid is $\frac{\partial \mathbf{u}}{\partial t} + (\mathbf{u} \cdot \nabla)\mathbf{u}$.

$$ma = \left(\frac{\partial \mathbf{u}}{\partial t} + (\mathbf{u} \cdot \nabla)\mathbf{u}\right)\rho\delta V$$

Utilizing the fact that $F = ma$, a slight reordering yields the first of Euler's equations:

$$\frac{\partial \mathbf{u}}{\partial t} + (\mathbf{u} \cdot \nabla)\mathbf{u} = -\nabla \frac{p}{\rho} + g \tag{1}$$

$$\nabla \cdot \mathbf{u} = 0 \tag{2}$$

Equation (2) follows from conservation of an incompressible fluid mass entering and displacing the existing fluid in the small volume.

Irrotational Flow

An irrotational flow is one with vorticity, the curl of velocity, equal to zero.

$$\nabla \times u = 0$$

Assuming irrotational flow, along with the ideal fluid assumption, simplifies the Euler equations (1) - (2) and provides a widely accepted model for water waves [28]. First, if using a velocity potential, ϕ, where $\mathbf{u} = \nabla\phi$, note that from equation (2), the velocity potential must satisfy Laplace's equation, $\nabla^2\phi = 0$, in the entire domain of the fluid.

Further, $(\mathbf{u} \cdot \nabla)\mathbf{u} = (\nabla \times u) \times u + \nabla(\frac{1}{2}u^2)$ which reduces to $\nabla(\frac{1}{2}u^2)$ for irrotational flows. This means that equation (1) becomes

$$\phi_t + \frac{1}{2}\left(\phi_x^2 + \phi_y^2 + \phi_z^2\right) + g\eta - \tau\kappa(\eta) = 0 \tag{3}$$

in terms of the velocity potential on the free-surface boundary, $\eta(x, y, t)$. Note that τ is the surface tension constant and κ curvature from the pressure on the boundary.

We also define a quantity, $f(x, y, z, t) = z - \eta(x, y, t)$, which is equal to zero on the boundary (i.e., $z = \eta$). Under the assumption that fluid particles on the free surface remain on the surface, which is reasonable if the boundary interface is not turbulent

and breaking, the time derivative of f will also be zero on the boundary. Then via the chain rule:

$$\frac{Df}{Dt} = \frac{\partial f}{\partial x}\frac{\mathrm{d}x}{\mathrm{d}t} + \frac{\partial f}{\partial y}\frac{\mathrm{d}y}{\mathrm{d}t} + \frac{\partial f}{\partial z}\frac{\mathrm{d}z}{\mathrm{d}t} + \frac{\partial f}{\partial t} = 0 \tag{4}$$

In order to express equation (4) in terms of the velocity potential and the free-surface, note that:

$$\frac{\mathrm{d}x}{\mathrm{d}t} = u = \phi_x, \quad \frac{\mathrm{d}y}{\mathrm{d}t} = v = \phi_y, \quad \frac{\mathrm{d}z}{\mathrm{d}t} = w = \phi_z \tag{5}$$

and the derivatives of f are:

$$\frac{\partial f}{\partial x} = -\eta_x, \quad \frac{\partial f}{\partial y} = -\eta_y, \quad \frac{\partial f}{\partial z} = 1, \quad \frac{\partial f}{\partial t} = -\eta_t \tag{6}$$

Together, equations (4) - (6) direct that the fluid interface is governed by what is known as the kinematic equation on the free-surface:

$$\eta_t + \eta_x\phi_x + \eta_y\phi_y = \phi_z \tag{7}$$

Euler's Equations of Potential Flow

Combining Laplace's equation, a condition that the vertical component of the velocity is zero on the bottom boundary, H, the kinematic equation (7), and equation (3) these yield the following system:

$$\nabla^2\phi = 0, \qquad z < \eta \tag{8}$$

$$\phi_z = 0, \qquad z = H \tag{9}$$

$$\eta_t + \eta_x\phi_x + \eta_y\phi_y = \phi_z, \qquad z = \eta \tag{10}$$

$$\phi_t + \frac{1}{2}\left(\phi_x^2 + \phi_y^2 + \phi_z^2\right) + g\eta - \tau\kappa(\eta) = 0, \qquad z = \eta \tag{11}$$

In this system, equation (11) is known as the Bernoulli equation or as the dynamic boundary condition on the free surface. Note that H taken to be much smaller than

the horizontal length of the periodic wave is typically referred to as the shallow-water case, while $H \to -\infty$ is known as the deep-water case.

Vortex Sheet Formulation

Waves on an air/water interface can be considered a simplification of the more general vortex sheet problem [29]. Consider two fluids as occupying two domains, Ω_1, Ω_2, with the less dense fluid typically taken to be on top of the other. The fluid flows are irrotational, but each will have its own different, continuous velocity and velocity potential. Therefore, they will each satisfy Euler's equations in their respective domains. There is an additional relationship, as the pressure exerted normal to the boundary interface, S, must be equal on both domains. If not, one fluid would either push into the other or, if the pressures were opposite, separate. This yields the following system for $i = 1, 2$:

$$\frac{\partial \mathbf{u_i}}{\partial t} + (\mathbf{u_i} \cdot \nabla)\mathbf{u_i} = -\nabla \frac{p_i}{\rho_i} + g \qquad \text{in } \Omega_i \tag{12}$$

$$\nabla \cdot \mathbf{u_i} = 0 \qquad \text{in } \Omega_i \tag{13}$$

$$\hat{\mathbf{n}} \cdot \mathbf{u_1} = \hat{\mathbf{n}} \cdot \mathbf{u_2} \qquad \text{on } S \tag{14}$$

where $\hat{\mathbf{n}}$ is the normal vector to the interface S arbitrarily chosen to point into one domain.

While the normal velocities are equal as seen in Equation (14), a discontinuity of the tangential velocity on the boundary interface can occur, resulting in an infinite $\nabla \times u$. The interface, S, is known as the vortex sheet and the jump in tangential velocities, $[\mathbf{u}]_2^1$, gives the value $\boldsymbol{\mu} = \hat{\mathbf{n}} \times [\mathbf{u}]_2^1$, known as the vortex sheet strength.

1.4 Free-Surface Problem

A complication in the fluid wave problem is that the boundary is unknown. Moreover, the interface is the boundary of the domain over which the potential is solved. One is required to solve for the potential simultaneously with the domain over which the potential is defined. There are several different techniques to solve the two-dimensional free-boundary problem.

Stokes expansion is the classic method first employed by G.G. Stokes [9]. Numerical calculations using this expansion can suffer from machine-precision errors. Recently, the method of Transformed Field Expansion (TFE) was introduced by Nicholls [3] to alleviate these errors. TFE is useful on both two- and three-dimensional fluids [30], but does not allow for overturning waves [23].

Dirichlet-to-Neumann operators (DNO) [31, 32] are another distinct method of solution. Dirichlet data pertains to the function itself at the surface, while Neumann data pertains to the function's derivative on the surface. A summary of computations of DNO methods for the water wave problem was done by Wilkening [33].

The Ablowitz, Fokas and Musslimani (AFM) Method [34] is a recent method that removes the vertical component from the formulation. AFM converts the usual Euler's equations, (8) - (11), into an integro-differential equation to determine the boundary interface. Extensions of AFM to include overturned traveling waves are currently being pursued in two-dimensions by Oliveras [35].

Conformal mapping has been used to solve water wave problems by numerous groups, most relevant to our work is that of Milewski and Wang [1]. This mapping is extremely efficient, allows for overturning waves, and requires very few numerical points. It handles the unknown domain by mapping the fluid domain of a two-dimensional problem onto a half-plane. In this way, the free-surface becomes fixed. Unfortunately, this method does not have a three-dimensional extension.

The model primarily focused on in this dissertation is a vortex sheet formulation. This is an interface model with a system of evolution equations for the interface location and vortex sheet strength. The system is coupled with an equation for the fluid velocity, $\boldsymbol{W}$, which is either the full term (the Birkhoff-Rott integral) or a "small-scale" approximation. While not quite as efficient as conformal mapping, this method is still tractable in a one-dimensional interfacial system. On the one-dimensional interface discretized by N points, the cost of computing the full $\boldsymbol{W}$ is $O(N^2)$ while for small-scale it is $O(NlogN)$. The three-dimensional vortex sheet system is a straight forward extension, as seen in the work of Akers and Reeger [26]. For the full $\boldsymbol{W}$ though, the cost jumps to $O(N^4M^2)$ with N being the number of points in each lateral direction and M a number of truncated terms of a summation. The small-scale approximation has a clear computational advantage at a cost of $O(N^2\log(N^2))$.

As direct numerical simulation of the full three-dimensional vortex sheet is extremely expensive, we design a numerical continuation procedure called dimension-breaking continuation in an effort to reduce computational requirements. Before extending to the three-dimensional solver, a new two-dimensional solver of the linearized system is proposed to accurately predict the bifurcation period of planar waves, thereby reducing the number of computations spent working in the fully three-dimensional model.

1.5 Traveling Wave Solutions

In this work, we consider traveling solutions of wave equations moving at a steady speed, c, in the x-direction. We use a traveling frame of reference so that the wave becomes stationary in the frame. For functions of x, t, a traveling wave ansatz $f(x,t) = f(x-ct)$ is used, yielding $f_t = -cf_x$. In the Euler equations of potential flow, this is substituted into the kinematic (10) and dynamic (11) equations

removing time-dependence. Several models used in this dissertation will utilize this substitution. However, waves that are overturned are of current interest in the field. These waves are therefore no longer functions of x, so this ansatz will have limited use.

To overcome this difficulty, the vortex sheet formulation used by Akers, Ambrose and Wright [25] parameterizes the one-dimensional surface and Akers and Reeger [26] parameterize the two-dimensional surface. Here and throughout this dissertation, subscript numbers are a naming convention to designate different functions. Sometimes this helps differentiate between similar functions in differing spatial directions, e.g. tangent vectors t_1, t_2, and sometimes it helps distinguish functions at different perturbation orders, e.g. x_0, x_1. Subscript variables, e.g. u_x or X_α, indicate derivatives in the subscripted variable. If both subscripts are being used, the different subscripts will be separated by parenthesis, e.g. $(u_0)_{xx}$, or a comma $u_{0,xx}$. In those examples, we are taking the second x derivative of the function u_0. Superscript numbers in paranthesis, e.g. $X^{(2)}$, indicate entry of a vector.

Following the work of Akers and Reeger [26], a curve is parameterized as $(x(\alpha,\beta,t), y(\alpha,\beta,t), z(\alpha,\beta,t))$, with unit tangent vectors, $\hat{t}_1, \hat{t}_2$ in the α and β directions. These are defined to be the α and β derivatives of the position functions x, y, z normalized to length 1. The choice of normal direction is arbitrary as long as it is maintained throughout the system. Here, the unit normal vector is $\hat{n} = \hat{t}_1 \times \hat{t}_2$. Then the curve translates with tangential velocities, V_1, V_2, and normal velocity, U, so that:

$$\begin{pmatrix} x \\ y \\ z \end{pmatrix}_t = U\hat{n} + V_1\hat{t}_1 + V_2\hat{t}_2 \tag{15}$$

from which we will have time-based evolution equations of the curve. Rewriting the

right-hand side as a matrix-vector multiplication and imposing the speed c in the x-direction on the left-hand side for traveling wave solutions, we have:

$$\begin{pmatrix} c \\ 0 \\ 0 \end{pmatrix} = \begin{pmatrix} & & \\ \hat{n} & \hat{t}_1 & \hat{t}_2 \\ & & \end{pmatrix} \begin{pmatrix} U \\ V_1 \\ V_2 \end{pmatrix} \tag{16}$$

As the normal and tangent vectors are orthonormal to each other, they form a unitary matrix. Therefore, the matrix is invertible by a simple transpose and

$$\begin{pmatrix} & \hat{n} & \\ & \hat{t}_1 & \\ & \hat{t}_2 & \end{pmatrix} \begin{pmatrix} c \\ 0 \\ 0 \end{pmatrix} = \begin{pmatrix} U \\ V_1 \\ V_2 \end{pmatrix} \tag{17}$$

For traveling waves, this imposes the restrictions $U = cn^{(1)}, V_1 = ct_1^{(1)}$ and $V_2 = ct_2^{(1)}$.

1.6 Dimension-Breaking Bifurcations

Dynamical systems often have points where the solution branch splits. These are termed bifurcation points, and were first noted by Poincare in 1885 [36]. We are studying an infinite-dimensional dynamical system whose equilibria are functions. The bifurcations we seek are those where a solution is trivial in one spatial dimension, then gains non-trivial transverse dependence.

This phenomenon is referred to as dimension-breaking and has been studied for some water wave models [13, 26, 4]. Using dimension-breaking as a tool to move from a lower-dimensional model to a higher-dimensional model will reduce the number of calculations required in the higher-dimensional solver and thereby increase computational efficiency.

II. Numerical Methodology

2.1 Dimension-Breaking Continuation Procedure

Dimension-breaking continuation is not limited to interfacial flows, and so the procedure is presented in a general way. In order to compute a large amplitude (N+1)-dimensional solution, the following procedure is proposed:

- Begin with a fully (N+1)-dimensional model, $F(x_1, \ldots, x_{N+1}) = 0$ that allows for planar solutions, which are trivial in the transverse direction, $x_{N+1} = \tilde{x}_{N+1}$.
- Separate out the N-dimensional problem, $F(x_1, \ldots, x_N, \tilde{x}_{N+1}) = 0$.
- Solve the N-dimensional problem via a quasi-Newton method.

  - Using numerical continuation, find a N-dimensional solution branch.

- Define a weakly-(N+1)-dimensional ansatz with small ε perturbations. The search direction for the (N+1)-dimensional solver is comprised of the perturbation functions and bifurcation parameters of the ansatz.
- Linearize the problem with the ansatz and group $O(\varepsilon)$ terms.
- Solve for the search direction in the $O(\varepsilon)$ terms.
- Solve (N+1)-D problem.

  - Extend N-D solution to (N+1)-D planar solutions. These trivial extensions exactly solve (N+1)-D system.

  - Initialize the (N+1)-dimensional quasi-Newton solver with the search direction and ansatz.

  - Use numerical continuation in fully (N+1)-D solver.

Note that there is no difference proposed for either the N- or (N+1)-dimensional solvers in this procedure. Using this method to understand the bifurcation structure and solving the linearization allows one to use the lower-dimensional (and thereby fast relative to the higher-dimensional) solver first to compute planar solutions of large amplitude. By continuing up the N-dimensional branch of solutions before starting any fully (N+1)-dimensional calculations, computational savings are achieved.

2.2 Fourier Basis

This study focuses on bifurcations from one- to two-dimensional wave interfaces in three different interfacial fluid flow models. One-dimensional solitary waves or wave packets are numerically truncated and so can be estimated as periodic waves, and all models are periodic in the transverse direction. Limiting numerical code to search for smooth periodic solutions makes a Fourier basis the natural choice. This study utilizes a Fourier collocation method to find the Fourier modes of wave interfaces.

In order to take computational advantage of the Fast Fourier Transform (FFT) the domain is discretized evenly with N points, where $N = 2^m, m \in \mathbb{N}$. The discretization allows for the FFT and IFFT to use $O(N\log N)$ operations instead of $O(N^2)$. An early portion of this study considered using adaptive discretization, however as the waves are periodic and smooth there was no significant advantage.

Additionally, even functions have Fourier modes with only real values, whereas odd functions have only imaginary Fourier modes. All real-valued functions' Fourier modes are also even. By enforcing the even or odd parity of the functions of the wave solution and conducting parity analysis, the number of unknowns in the numerical code will be reduced.

2.3 Quasi-Newton Solvers

The dimension-breaking continuation procedure utilizes three distinct solvers in order to find the Fourier modes. First, a solver is used for the N-dimensional wave interface, then another finds the appropriate search direction, and finally a solver generates fully (N+1)-dimensional wave solutions.

An initial goal of this study was to use an eigensolver in order to define a valid search direction. An eigensolver could be directly applied to a one-dimensional interface anywhere along the branch of solutions, a significant advantage over a quasi-Newton solver that requires an initial guess. If the bifurcation period had an asymptote, the eigensolver could skip past it and continue.

In two of the three models studied, the bifurcation parameter, d, of the search direction appeared as a linear operator. This allowed for the linearization to take on the form of an eigenvalue problem and the search direction to be successfully solved with the use of an eigensolver.

In a class of models where the bifurcation parameter, d, is embedded in non-linear terms though, the linearization is no longer an eigenvalue problem. The third model studied was of this form and for this reason, a quasi-Newton method was ultimately required to solve for the search direction.

The disadvantage of the quasi-Newton solver over an eigensolver for the dimension-breaking linearization is that it requires an initial guess. It is presently coded to work concurrently with the one-dimensional traveling wave solver. After each one-dimensional interface solution is calculated, the bifurcation period and perturbations are solved with an initial guess of the previous dimension-breaking solution. This method requires bifurcation periods to have continuous dependence on height.

Quasi-Newton solvers were also used for all one- and two-dimensional wave interfaces. In a quasi-Newton solver, one immediate advantage of using Fourier col-

location is the size of the Jacobian. Quasi-Newton methods require a full Jacobian at every step. As mentioned in the last section, only half of the Fourier modes of one-dimensional real-valued solutions need to be stored. The entire function can be recreated by reflecting the stored modes appropriately based on the function's parity. This reduces the Jacobian size from $(N+1)^2$ to $(N/2+1)^2$. A two-dimensional surface requires only one quarter of the Fourier modes to be stored.

Our code uses a numerical approximation of the Jacobian's partial derivatives via symmetric difference of plus or minus step size h. The fully two-dimensional interface solver utilizes a Broyden's update [48] to control computational time and storage issues for the Jacobian. Broyden's updates are not required in the one-dimensional dimension-breaking solvers.

2.4 Numerical Continuation

As stated earlier, quasi-Newton solvers require an initial guess to get started. After a solution is found, a small change to the problem can be made such as enforcing a slightly larger amplitude. The quasi-Newton solver can be reapplied with the new constraint and the previously found solution as an initial guess. By repeatedly solving a mathematical model in this way, one can march up a branch of solutions. This general technique is known as numerical continuation and is referenced often throughout this work. It is used in the one- and two-dimensional interface solvers of this dissertation as well as in the dimension-breaking continuation procedure.

III. Dimension-Breaking Method in Weakly-Nonlinear Models

Dimension-breaking has been demonstrated in several different wave equations [13] including bifurcating from solutions of the Korteweg-deVries equation to those of the Kadomsev-Petviashvili equation. The KdV equation has exact solutions available to compare against computational output and the bifurcation parameter to solutions of the KP equation is well understood [15, 4]. For these reasons, the KdV to KP bifurcation was used in this research to demonstrate the effectiveness of the dimension-breaking continuation procedure.

3.1 The Korteweg-deVries and Kadomtsev-Petviashvili Equations

The Korteweg-deVries equation for a line traveling wave is as follows:

$$u_{xxx} - cu_x - 3uu_x = 0 \tag{18}$$

with the exact solution $u = -c\ \mathrm{sech}^2(\sqrt{c}\ x/2)$.

Kadomtsev and Petviashvili proposed the following equation as an analogue of the KdV equation to find two-dimensional surface wave solutions [14]

$$(u_{xxx} - cu_x - 3uu_x)_x + u_{yy} = 0 \tag{19}$$

A solution to the KdV equation in the x direction that is extended homogeneously in the transverse, y, direction will be a solution to the KP equation. An explicit formula for fully two-dimensional KP waves was proposed by Tajiri and Murakami [15] and rigorously analyzed for wave speed $c = 1$ by Groves et. al. [4]:

$$u(\delta, x, y) = -\frac{4(1-\delta^2)}{4-\delta^2}\frac{1-\delta\cosh(\alpha^\delta x)\cos(\omega^\delta y)}{(\cosh(\alpha^\delta x)-\delta\cos(\omega^\delta y))^2} \tag{20}$$

where

$$\alpha(\delta) = \sqrt{\frac{1-\delta^2}{4-\delta^2}} \qquad \text{and} \qquad \omega(\delta) = \frac{\sqrt{3(1-\delta^2)}}{4-\delta^2} \tag{21}$$

At $\delta = 0, u$ reduces to the KdV solution. Varying $\delta \in [0, 1)$ yields exact KP solutions bifurcating from the transversely trivial state. Note that in Equation (20), the transverse parameter, δ, defining the bifurcation period changes while the speed remains stable at $c = 1$. For our numerical coding purposes, we will instead fix the transverse period and allow the speed to change.

Results

In applying the dimension-breaking procedure to the KP equation (19), the following ansatz was used:

$$u(x, y) = u_0(x) + \varepsilon u_1(x)\cos(dy) \tag{22}$$

where u_0 is a solution to the KdV equation (18) from which we wish to bifurcate to KP waves. This ansatz was chosen to be periodic in the transverse y direction, with $\varepsilon \ll h = \max(u_0) - \min(u_0)$.

Linearizing the KP equation with this ansatz results in an equation with an $O(1)$ piece that is solved exactly by u_0, and an $O(\varepsilon)$ piece of the form $A(u_1) = \lambda u_1$ where

$$A(u_1) = (u_1)_{xxxx} - c(u_1)_{xx} - 6(u_0)_x(u_1)_x - 3(u_0)(u_1)_{xx} - 3(u_0)_{xx}(u_1)$$

and $\lambda = d^2$.

In order to solve for $[u_1, d]$ pairs numerically, the functions are discretized with N points. The operator A is then calculated as an $N \times N$ matrix and an eigensolver, such as MATLAB's eig() function, is applied. Afterwards, the eigenvalues, d, are sorted to find smallest $d \in \mathbb{R}^+$. Figure 1 shows an example of a KdV wave, u_0, and the perturbation function, u_1, calculated from the dimension-breaking continuation procedure.

The $[u_1, d]$ pair constitutes a search direction in a quasi-Newton solver for the KP equation by defining the transverse period, $Ly = 2\pi/d$, and as the initial guess in the ansatz equation (22). After a KP wave solution is found, numerical continuation as described in Section 2.4 is used to increase the amplitude of the wave.

The Speed/Amplitude plot for this model is seen in Figure 2. It shows the planar wave branch in solid blue as computed with the more efficient one-dimensional KdV interface model. A dimension-breaking bifurcation line in dashed red originates from a planar wave.

Continuation on this branch was suspended at a height of $h = 2.37$ as marked by the black star of Figure 2. The fully two-dimensional KP interface generated using this procedure is seen in Figure 3.

In this model, the transverse bifurcation parameter, d, was computed for KdV waves between speeds 0.2 and 3 and compared against the explicit formula provided in [4]. For the KdV to KP bifurcations, it is a linear relationship, $d = c\sqrt{3}/4$, as seen in Figure 4.

The bifurcation parameter, d, need not have simple amplitude dependence. For example, initial studies of the aspect ratio of the x, y periods for Meiron-Saffman waves (standing gravity-capillary waves in deep water) have yielded the graph in Figure 5 for the bifurcation period (here denoted as $Ly = 2\pi/d$). As the height increases, the bifurcation period contains a minimum and then begins to increase. While an explicit

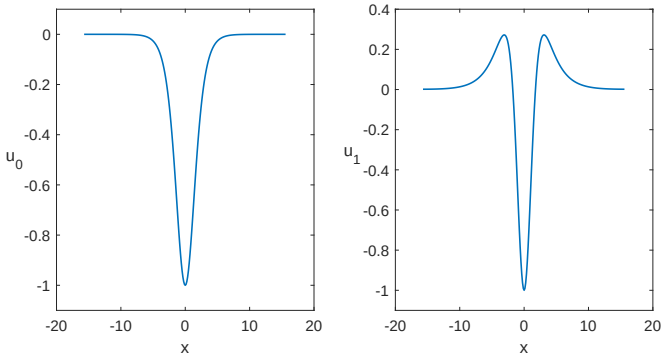

Figure 1. Example of a starting KdV wave interface, u_0, from Equation (18) with wave speed $c = 1$ at left, and solved u_1 perturbation, right, paired with bifurcation parameter $d = 0.433$. Note that these are solitary waves over the whole real line, truncated for numerical computation.

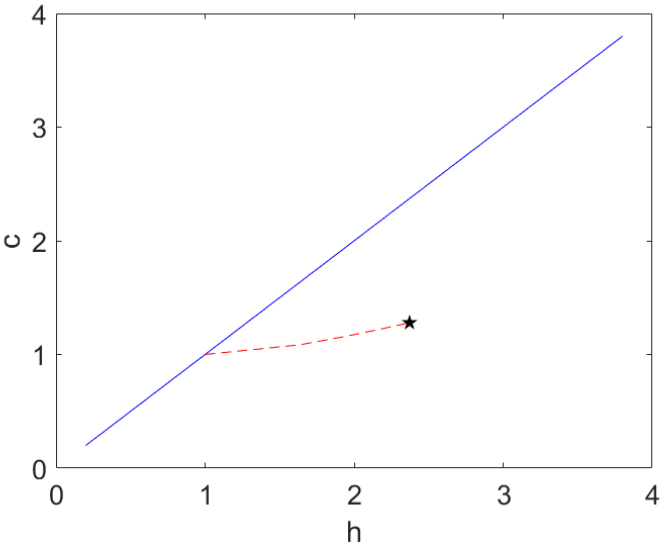

Figure 2. Speed/Amplitude plot. c is the wave speed and the amplitude $h = \max(u) - \min(u)$. The solid blue line is from KdV solutions extended to planar waves. The bifurcation begins at $c = 1$ and continues, red dashed line, as a fully two-dimensional wave surface solution of the KP equation.

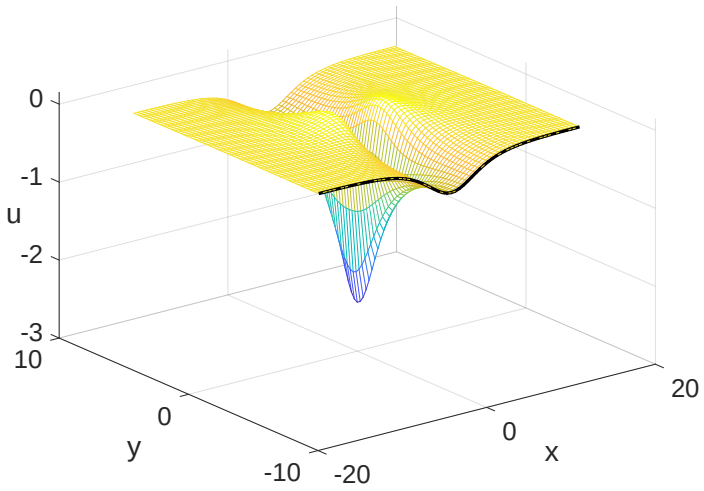

Figure 3. A traveling KP wave, location denoted in Figure 2 by the star, calculated using the dimension-breaking procedure.

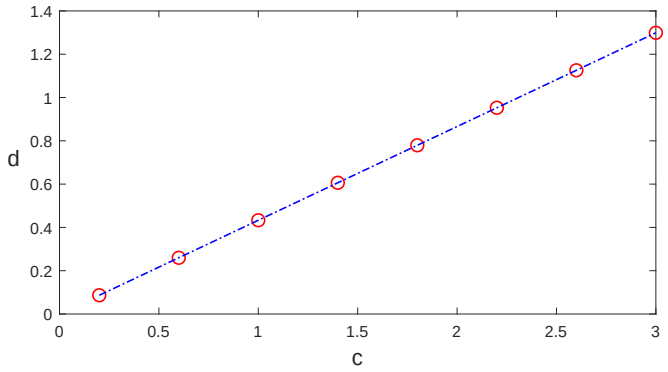

Figure 4. Linear relationship of transverse bifurcation parameter, d, in the KP equation (19) to wave speed, c. Computed results, red circles, are compared against expected values from the explicit formula provided by Groves et. al. [4], blue dashed line.

equation for the bifurcation parameter exists for KdV to KP bifurcations, there is a need for a procedure to identify the appropriate bifurcation period for other models.

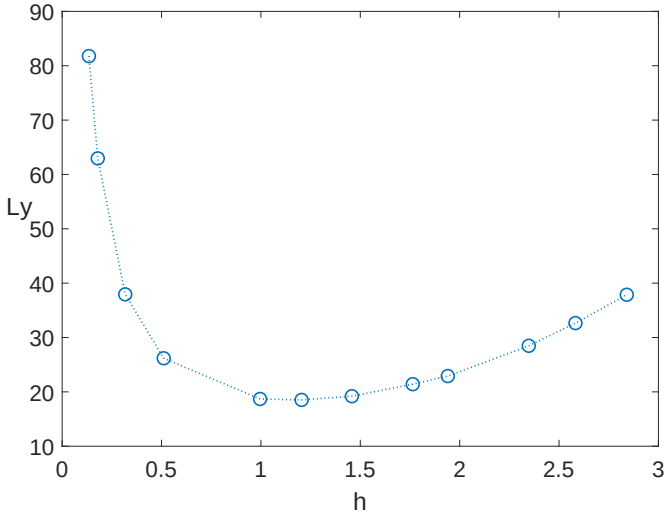

Figure 5. Bifurcation periods, $Ly = 2\pi/d$, in the y axis arising from planar Merion-Saffman waves ($g = 1, \tau = 0,$ At $= 0.1$ in a vortex sheet formulation, equations (24)-(27)), plotted against $h = \max(z) - \min(z)$, the amplitude of the wave.

3.2 The Akers-Milewski Equation

Next, we apply the procedure to another interfacial fluid flow model, the Akers-Milewski (AM) equation, first proposed in [37] and later compared to experiment in [38]:

$$-cu_x + \mathcal{H}u + 2u_x - \mathcal{H}u_{xx} - \frac{3}{2}uu_x + 2\mathcal{H}u_{yy} = 0 \tag{23}$$

where $\mathcal{H}$ is the Hilbert Transformation in the x-direction. This is another evolution equation with a traveling wave ansatz applied, similar to the KP equation. Note that the Hilbert Transform is an operator on the Fourier representation of a function, with Fourier symbol

$$\widehat{\mathcal{H}}(u(x)) = -i\ \mathrm{sign}(k)\widehat{u(x)}$$

in which $\widehat{\mathcal{H}}$ refers to the Fourier transform of $\mathcal{H}$, k is the wavenumber and $i = \sqrt{-1}$. A one-dimensional wave interface from the AM model with speed $c = 0.3$ is seen in Figure 6.

The Hilbert Transformations in this model did not affect the procedure or ansatz. This transformation is a linear operator and the bifurcation parameter, d, remained separable into the form of an eigenvalue problem. An eigensolver is still a viable method of solving for the transverse bifurcation periods and perturbation functions. A plot of the calculated bifurcation periods, Ly, can be seen in Figure 8. Additionally, Figure 9 shows a log-log plot of the bifurcation periods along with a reference line for the small-amplitude asymptotic, $O(1/h)$. Milewski and Wang [39] studied the small-amplitude asymptotic for a nonlinear Schrödinger formulation that supports wave packets visually similar to solutions of the AM equation. Their study also yielded an asymptotic of $O(1/h)$.

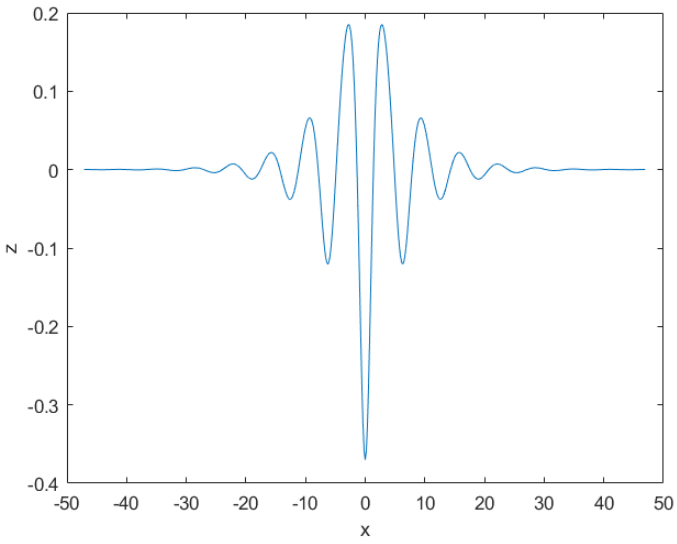

Figure 6. An AM traveling wave, u_0, with speed $c = 0.3$, computed using a quasi-Newton method with N=256 points.

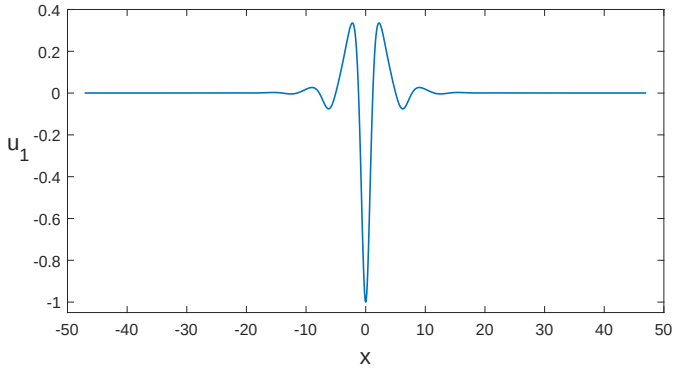

Figure 7. An AM perturbation wave, u_1 generated for the u_0 wave in Figure 6.

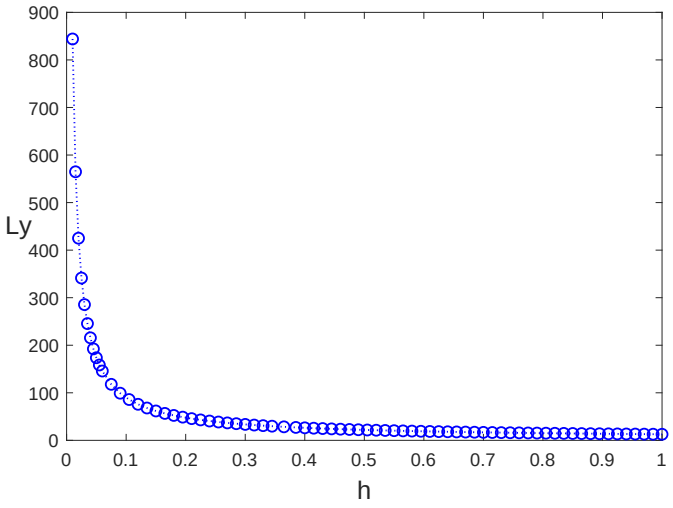

Figure 8. Bifurcation periods, $Ly = 2\pi/d$, of the Akers-Milewski equation (23) plotted against height $h = \max(u) - \min(u)$ generated for several 2-D AM waves.

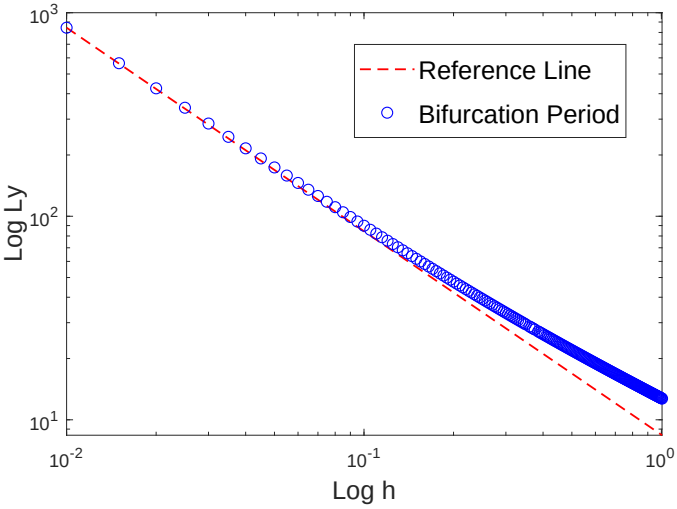

Figure 9. Log-log plot of bifurcation periods, $Ly = 2\pi/d$, plotted against height $h = \max(u) - \min(u)$, blue circles, for the AM equation (23). The reference line, red dashed line, is $O(1/h)$ to compare the deviation away from the small-amplitude asymptotic.

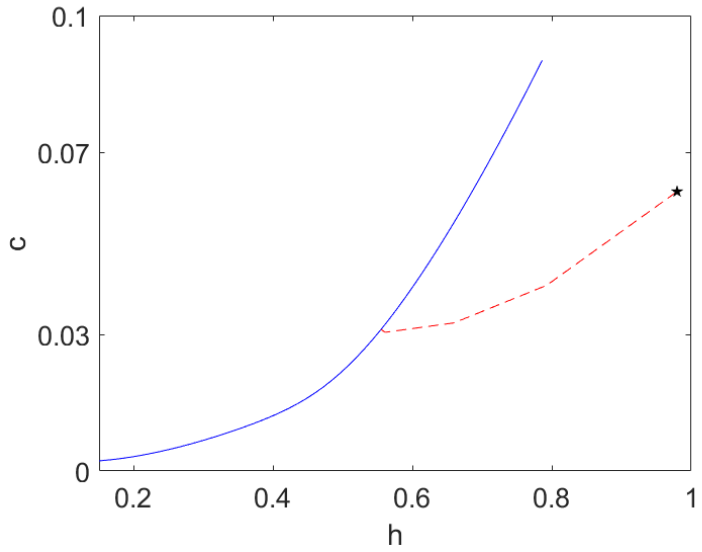

Figure 10. Speed/Amplitude plot for solutions of the AM equation (23)**.** c **is wave speed and the amplitude** $h = \max(u) - \min(u)$**. The solid blue line is data from one-dimensional interfaces. A bifurcation, red dashed line, of fully two-dimensional AM surface interfaces begins at speed** $c = 0.03$**.**

Note that the solid blue line Speed/Amplitude plot, Figure 10, is no longer linear or explicitly known in the AM model, as compared to the previous KdV model. Further, the bifurcation periods of Figure 8 do not have an explicit formula and, as seen in Figure 9, deviate from the small amplitude asymptotic. This illustrates the need for a method of finding the bifurcation parameter. The dimension-breaking continuation procedure provides this parameter and search direction accurately in order to begin solving for the fully two-dimensional surface interface.

Figure 11 shows a fully two-dimensional AM surface interface generated using this procedure. Bifurcations have been computed from many one-dimensional wave heights (figures not included, as they are visually similar to the one provided), suggesting that the bifurcations exist continuously along the branch. The wave interfaces generated are as expected from the previous work of Akers and Milewski [37].

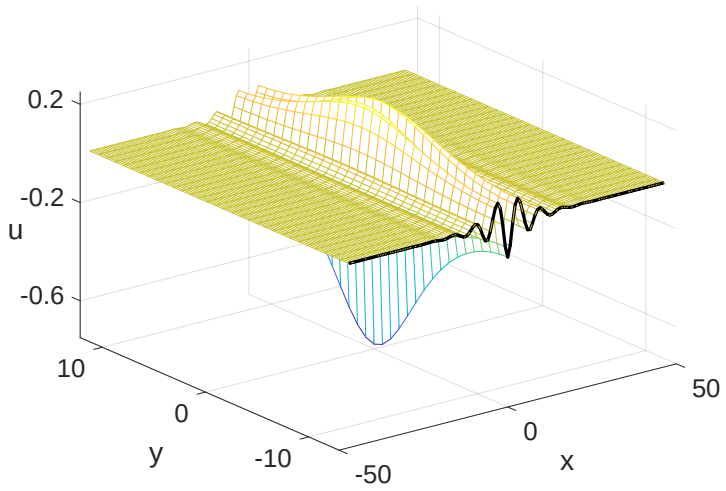

Figure 11. A traveling wave solution of the AM equation (23), location denoted on the Speed/Amplitude plot of Figure 10 by the star, calculated using the dimension-breaking procedure.

IV. Vortex Sheet Model

Computations of the two-dimensional interfaces of the AM or KP equations have been shown to work using the dimension-breaking continuation procedure. The AM and KP models do not support overturned traveling waves (and cannot since they are parameterized in x). Next we proceed to an approximation of the vortex sheet equations, so as to evaluate the potential for dimension-breaking continuation in this context.

First, the model used by Akers and Reeger in [26] is presented. A fluid velocity closure is required in this system. The full vortex sheet equations contain a Birkhoff-Rott integral but, as it is computationally expensive, Akers and Reeger used the small-scale approximation of the integral in their work. This study instead uses a reduced small-scale approximation, discussed in Section 4.4.

4.1 Model

As stated generally in Section 1.3, the vortex sheet formulation is used to model two fluids and an interface between them. The fluids occupy distinct domains and do not mix or push into each other. In their respective domains the fluid velocities are continuous, but on the interface a velocity shear may exist. Vortex sheets are used to model fluids of different densities, such as ocean water of differing salinity or oil on top of water. Additionally, discontinuous interfacial flow velocities can arise in airflow beyond the sharp edge of a wing or on either side of a flapping flag [40].

The vortex sheet system in this study contains four equations: an evolution equation of the vortex sheet strength, μ; an evolution equation for the velocity of the wave

interface; and two isothermal parameterization equations.

$$0 = \tau\kappa + \frac{1}{\sqrt{E}}\left(\boldsymbol{V}\cdot\nabla\right)\mu + \mathrm{At}\left(|W|^2 + 2W\cdot\boldsymbol{t}_1 V_1 + 2W\cdot\boldsymbol{t}_2 V_2 - \frac{1}{4E}\left|\nabla\mu\right|^2 - 2gz\right) \tag{24}$$

$$0 = c(\boldsymbol{n})^{(1)} - W\cdot\boldsymbol{n} \tag{25}$$

$$0 = X_\alpha \cdot X_\beta \tag{26}$$

$$0 = E - \lambda G \tag{27}$$

where τ is surface tension, κ is the curvature of the interface and g is the constant force due to gravity. The Atwood number, $\mathrm{At} = \frac{\rho_1-\rho_2}{\rho_1+\rho_2}$, is a difference of the densities, ρ_1, ρ_2, of the two fluids. $X = (x, y, z)$ is the wave interface, and G and E are fundamental forms $E = X_\alpha \cdot X_\alpha$, $G = X_\beta \cdot X_\beta$, with λ a ratio of the α and β parameterizations. Tangent vectors to the interface are $\boldsymbol{t}_1 = X_\alpha/||X_\alpha||$ and $\boldsymbol{t}_2 = X_\beta/||X_\beta||$. The normal vector to the interface is $\boldsymbol{n} = \boldsymbol{t}_1 \times \boldsymbol{t}_2$. The system is coupled with a fluid velocity closure, W, discussed in the next section.

The first equation (24) of the system is the evolution equation of μ. As we are seeking traveling wave solutions, the vortex sheet strength will be static in the traveling frame and hence the left hand side is zero. The second equation (25) is the kinematic equation. It is a reduction that seeks traveling waves with steady speed c in the x-direction of the full kinematic equation, $X_t = U\boldsymbol{n} + V_1\boldsymbol{t}_1 + V_2\boldsymbol{t}_2$.

The isothermal parameterization will be preserved via equations (26) and (27) in line with the work of Ambrose, Siegel, and Tlupova [41, 42]. Equation (26) is referred to as the perpendicular equation and enforces that the parameterization locally maintains right angles between α, β, and equation (27) is the aspect equation and is a relationship of the average arc length in the α and β directions. The equations allow for general λ, however we will be assuming $\lambda = 1$ throughout this study.

4.2 The Birkhoff-Rott Integral

The Birkhoff-Rott equation, W, gives the velocity induced on the fluid flow in the vortex sheet formulation. This section will present the derivation of the full equation from previous works, however an approximation is used for this dissertation and is defined in the following sections.

Recall that there are two fluid domains, with the vortex sheet defining the boundary between them. Saffman's *Vortex Dynamics* [43] uses the Biot-Savart law to reduce from a general integral equation over the fluid domains to a surface integral on the vortex sheet:

$$\boldsymbol{u}(\boldsymbol{x},t) = \frac{1}{4\pi}\int_S \boldsymbol{\omega}(\boldsymbol{x}',t) \times \frac{\boldsymbol{x}-\boldsymbol{x}'}{|\boldsymbol{x}-\boldsymbol{x}'|^3} d\boldsymbol{x}' \tag{28}$$

where $\boldsymbol{u}$ the fluid velocity, $\boldsymbol{x}$ is a position vector in either fluid domain (not on the interface), $\boldsymbol{x}'$ is a position vector on the interface, and the vorticity is $\boldsymbol{\omega} = \nabla \times \boldsymbol{u}$. The fluid flows in both the upper and lower domains are assumed to be irrotational so that the vorticity is zero away from the interface, but on the sheet itself that is not the case.

The fluid velocities in each domain, $\boldsymbol{u}_1, \boldsymbol{u_2}$, are continuous but there is a velocity shear on the sheet itself. The average velocity across the shear, $\boldsymbol{U} = 1/2\,(\boldsymbol{u}_1 + \boldsymbol{u_2})$, is found following the derivation of Caflisch and Li [44]. They apply a limiting process with the Plemejl formula on either side of the boundary to define:

$$\boldsymbol{U}(\boldsymbol{x},t) = \frac{1}{4\pi} P.V. \int_S (\boldsymbol{n}' \times \nabla_\tau \phi') \times \frac{\boldsymbol{x}-\boldsymbol{x}'}{|\boldsymbol{x}-\boldsymbol{x}'|^3} ds(\boldsymbol{x}') \tag{29}$$

where $\boldsymbol{n}$ is the normal vector pointing from the sheet into the upper domain, ϕ is velocity potential, and the gradient of the sheet is $\nabla_\tau = \nabla\phi - (\boldsymbol{n}\cdot\nabla\phi)\,\boldsymbol{n}$.

Note that $\boldsymbol{x}$ is now on the interface, so there is a discontinuity where $\boldsymbol{x} = \boldsymbol{x}'$. The

P.V. indicates the surface integral will be a Cauchy Principal Value integral due to the discontinuity.

Cauchy Principal Value integrals allow for the evaluation of integrals with singularities on their domain of integration. For the one-dimensional interface of this particular integral (29):

$$P.V. \int_{-\infty}^{\infty} f(x')ds(x') = \lim_{\epsilon \to 0^+} \left(\int_{-\infty}^{x-\epsilon} + \int_{x+\epsilon}^{\infty} \right) f(x')ds(x') \tag{30}$$

This Principal Value integral is said to exist if the limit exists as ϵ approaches zero. A full discussion of Cauchy Principal Value integrals with singularities at a finite location can be found in [46].

The Birkhoff-Rott equation for fluid velocity on the sheet can come with some variation to fit the units of the system in which it is used. Ambrose [45], Akers and Reeger [26], Akers, Ambrose and Wright [25] parameterize the coordinates $\boldsymbol{X}(\alpha, \beta, t)$, so the following form will be used where $\boldsymbol{W}$ is the fluid velocity:

$$\boldsymbol{W}(\boldsymbol{X}) = \frac{1}{4\pi} P.V. \int\int \left(\mu_\alpha \boldsymbol{X}'_\beta - \mu_\beta \boldsymbol{X}'_\alpha \right) \times \frac{\boldsymbol{X} - \boldsymbol{X}'}{|\boldsymbol{X} - \boldsymbol{X}'|^3} d\beta' d\alpha' \tag{31}$$

Reduction of One-Dimensional Birkhoff-Rott Integral

Notice that the domain of integration of the Birkhoff-Rott integral equations (29) is the entire surface, from $-\infty$ to ∞, for a one-dimensional interface. This equation can be significantly reduced using the Mittag-Leffler cotangent identity [46]:

$$\frac{1}{2} \cot\left(\frac{v}{2}\right) = \sum_{m=-\infty}^{\infty} \frac{1}{(v - 2\pi m)} \tag{32}$$

Since we are interested in periodic wave solutions in this dissertation, generally where $x(\alpha + 2\pi) = x(\alpha)$, an integral over the whole real line can be expressed as an infinite

summation of integrals:

$$P.V. \int_{-\infty}^{\infty} \frac{f(\alpha)}{z(\alpha) - z(\alpha')} d\alpha' = \sum_{m \in Z} P.V. \int_{2\pi(m-1)}^{2\pi m} \frac{f(\alpha)}{z(\alpha) - z(\alpha')} d\alpha' \tag{33}$$

As in [29] the summation of the periodic function is able to be moved inside the integrand:

$$P.V. \int_{0}^{2\pi} \sum_{m \in Z} \frac{f(\alpha)}{z(\alpha) - z(a + 2\pi m)} da = P.V. \int_{0}^{2\pi} \sum_{m \in Z} \frac{f(\alpha)}{(z(\alpha) - z(a)) - 2\pi m)} da \tag{34}$$

and, applying the Mittag-Leffler identity, results in an integral of the form:

$$P.V. \int_{0}^{2\pi} \frac{f(\alpha)}{2} \cot\left(\frac{z(\alpha) - z(a)}{2}\right) da \tag{35}$$

This allows for the infinite sum over periodic images to be replaced with the evaluation of a trigonometric function.

The Mittag-Leffler identity is what allows the one-dimensional surface integral (29) to be computed efficiently at $O(N^2)$, and the absence of a two-dimensional analog of this identity is a significant computational bottleneck.

4.3 Small-Scale Approximation

Akers and Reeger [26] use a parameterized (α, β) surface Birkhoff-Rott integral, which is doubly-periodic:

$$\boldsymbol{W}(\boldsymbol{X}) = \frac{1}{4\pi} \sum_{n \in Z} \sum_{m \in Z} P.V. \int_{0}^{2\pi} \int_{0}^{\frac{2\pi}{k}} \left(\mu'_\alpha \boldsymbol{X}'_\beta - \mu'_\beta \boldsymbol{X}'_\alpha\right) \times \frac{\boldsymbol{X} - \boldsymbol{X}' - 2n\pi e_1 - \frac{2m\pi}{k} e_2}{\left|\boldsymbol{X} - \boldsymbol{X}' - 2n\pi e_1 - \frac{2m\pi}{k} e_2\right|^3} d\beta' d\alpha' \tag{36}$$

The cotangent identify of the previous section utilizes a map to $\mathbb{C}$ and has no

3-D analogue at this time to quickly evaluate the surface integral. This makes using the full Birkhoff-Rott integral computationally more difficult and significantly more expensive to evaluate for a three-dimensional fluid problem. If a two-dimensional surface is gridded by N points in each direction and each summation is truncated to M points, then every direct numerical evaluation of the integral will require $O(N^4M^2)$ calculations. As an intermediate model, an approximation [41, 47] has been used by Ambrose, Akers and Reeger. This approximation is termed the "small-scale" as it is asymptotically equivalent as it approaches the flat state:

$$W \approx \frac{1}{2} H_\alpha \left[-\frac{\mu_\alpha X_\beta \times X_\alpha}{E^{3/2}} \right] - \frac{1}{2} H_\beta \left[-\frac{\mu_\beta X_\alpha \times X_\beta}{E^{3/2}} \right] \tag{37}$$

where H_α, H_β are Reisz Transformations in α and β, expressed as differential operators $H_\alpha = -\partial_\alpha \left(-\partial_\alpha^2 - \partial_\beta^2\right)^{-1/2}$ and $H_\beta = -\partial_\beta \left(-\partial_\alpha^2 - \partial_\beta^2\right)^{-1/2}$. Using this small-scale approximation, the velocity field, W, is calculated using a Fast Fourier Transform, resulting in a cost of $O(N^2 \log(N^2))$ instead of the $O(M^2N^4)$ cost of the full Birkhoff-Rott equation.

4.4 Reduction of Small-Scale Approximation

For the purposes of this dissertation, a further reduction is being used by setting $W^{(1)} = 0$, which we will refer to as the "reduced small-scale". Both the small-scale and the reduced small-scale model have the same small amplitude asymptotic solution as the full vortex sheet equations. Both are also vector valued, contain Reisz transformations, and solve for a parameterized two-dimensional interface. Thus, the reduced small-scale model has the same increases in mathematical difficulty as the small-scale model over the weakly nonlinear models, the KP (19) and AM (23) equations.

Unlike the small-scale approximation, the reduced small-scale approximation does not support overturning waves. Dimension-breaking continuation is expected to be applied to the full small-scale approximation model in the author's future work.

4.5 Reisz Transformations

A major difficulty encountered in the vortex sheet model as compared to the weakly nonlinear models of Chapter 2 results from the Reisz Transformations in the Small-Scale approximation of the Birkhoff-Rott equation. The two-dimensional Reisz transformation acting on a function with two variables contains d dependence, unlike the Hilbert Transform encountered in the AM equation (23). The Reisz transformation is a pseudo-differential operator and as a result the d term cannot be isolated in an equation of the form $Au_1 = \lambda u_1$. Consequently, an eigensolver such as MATLAB's eig() function is no longer available as a method of solution.

A quasi-Newton solver can be used instead, at the expense of requiring an initial guess. The current method solves the dimension-breaking problem for each planar wave and uses the solution as the initial guess for the next larger wave. As the continuation is being conducted in the lower-dimensional system, the cost of the quasi-Newton solver for the dimension-breaking continuation still represents a significant savings over computations in the higher-dimensional system.

For the linearization ansatz in this model, the H_α operator will be evaluated only on two-dimensional functions of the form $f(\alpha, \beta) = v(\alpha)\cos(d\beta)$. Similarly, the H_β operator will be evaluated only on two-dimensional functions of the form $f(\alpha, \beta) = v(\alpha)\sin(d\beta)$.

For the dimension-breaking continuation method to remain efficient, calculations must not be required over the two-dimensional surface interface. By restricting the calculations to one dimension smaller than the full solver, the computational cost

is limited relative to the size of the full problem. Therefore, we desire to find how the operator acts on the function v and maintain a multiplication by $\cos(d\beta)$. The cosine term will be cancelled during the linearization. The following derivations were completed as part of this study.

Derivation of Applicable Reisz Transformations

The Reisz transforms have the following Fourier symbols:

$$\hat{H}_\alpha(f) = \frac{-ik_1}{\sqrt{k_1^2 + k_2^2}} \hat{f}(k_1, k_2)$$

$$\hat{H}_\beta(f) = \frac{-ik_2}{\sqrt{k_1^2 + k_2^2}} \hat{f}(k_1, k_2)$$

where the Fourier transform, $\hat{f}$, is

$$\hat{f} = \frac{1}{4\pi^2} \int_0^{2\pi} \int_0^{2\pi} f(\alpha, \beta) e^{-ik_1\alpha} e^{-ik_2\beta} d\alpha d\beta$$

and the inverse Fourier transform, $\check{f}$, is

$$\check{f} = \int_0^{2\pi} \int_0^{2\pi} f(k_1, k_2) e^{ik_1\alpha} e^{ik_2\beta} dk_1 dk_2$$

with k_1, k_2 wavenumbers in the α and β directions.

First, we will detail the calculations of the Riesz transform on functions of the form $f(\alpha, \beta) = v(\alpha)\cos(d\beta)$. We will use the complex exponential form of cosine for the manipulations, and then recover it back to $\cos(d\beta)$. These derivations to eliminate

the transverse variable, β, from the dimension-breaking continuation method:

$$\begin{aligned}
f(\alpha,\beta) &= v(\alpha)\cos(d\beta) = v(\alpha)\frac{e^{id\beta}+e^{-id\beta}}{2},\\
\hat{f} &= \frac{1}{4\pi^2}\int_0^{2\pi}\int_0^{2\pi} v(\alpha)\frac{e^{id\beta}+e^{-id\beta}}{2}e^{-ik_1\alpha}e^{-ik_2\beta}d\alpha d\beta\\
&= \frac{1}{4\pi^2}\int_0^{2\pi}\int_0^{2\pi} \frac{v(\alpha)}{2}e^{id\beta}e^{-ik_1\alpha}e^{-ik_2\beta}d\alpha d\beta\\
&\quad + \frac{1}{4\pi^2}\int_0^{2\pi}\int_0^{2\pi} \frac{v(\alpha)}{2}e^{-id\beta}e^{-ik_1\alpha}e^{-ik_2\beta}d\alpha d\beta\\
&= \frac{1}{4\pi^2}\int_0^{2\pi} \frac{v(\alpha)}{2}e^{-ik_1\alpha}d\alpha\int_0^{2\pi} e^{-i(k_2-d)\beta}d\beta\\
&\quad + \frac{1}{4\pi^2}\int_0^{2\pi} \frac{v(\alpha)}{2}e^{-ik_1\alpha}d\alpha\int_0^{2\pi} e^{-i(k_2+d)\beta}d\beta\\
&= \frac{\hat{v}}{2}\delta(k_2-d)+\frac{\hat{v}}{2}\delta(k_2+d)
\end{aligned}$$

Applying the Reisz Transformation in the α direction to functions of this form:

$$\begin{aligned}
\hat{H}_\alpha(v(\alpha)\cos(d\beta)) &= \frac{-ik_1}{\sqrt{k_1^2+k_2^2}}\left(\frac{\hat{v}}{2}\delta(k_2-d)+\frac{\hat{v}}{2}\delta(k_2+d)\right)\\
&= \frac{-ik_1}{\sqrt{k_1^2+d^2}}\hat{v}\left(\frac{\delta(k_2-d)}{2}+\frac{\delta(k_2+d)}{2}\right)
\end{aligned}$$

As the Dirac delta functions, δ, are zero except when $k_2 = \pm d$, this allows us to swap the k_2 term with d in the square root of the denominator of the first term. Now inverting the Fourier transform, we can recover the form containing $\cos(d\beta)$, so that:

$$H_\alpha(v(\alpha)\cos(d\beta)) = \left(\widetilde{\frac{-ik_1}{\sqrt{k_1^2+d^2}}\hat{v}}\right)\cos(d\beta)$$

Similarly for H_β, it will act on functions of the form $f(\alpha,\beta) = v(\alpha)\sin(d\beta)$:

$$
\begin{aligned}
f(\alpha,\beta) = v(\alpha)\sin(d\beta) &= v(\alpha)\frac{e^{id\beta}-e^{-id\beta}}{2i},\\
\hat{f} &= \frac{-i}{4\pi^2}\int_0^{2\pi}\int_0^{2\pi} v(\alpha)\frac{e^{id\beta}-e^{-id\beta}}{2}e^{-ik_1\alpha}e^{-ik_2\beta}d\alpha d\beta\\
&= \frac{-i}{4\pi^2}\int_0^{2\pi}\int_0^{2\pi}\frac{v(\alpha)}{2}e^{id\beta}e^{-ik_1\alpha}e^{-ik_2\beta}d\alpha d\beta\\
&\quad -\frac{-i}{4\pi^2}\int_0^{2\pi}\int_0^{2\pi}\frac{v(\alpha)}{2}e^{-id\beta}e^{-ik_1\alpha}e^{-ik_2\beta}d\alpha d\beta\\
&= \frac{-i}{4\pi^2}\int_0^{2\pi}\frac{v(\alpha)}{2}e^{-ik_1\alpha}d\alpha\int_0^{2\pi}e^{-i(k_2-d)\beta}d\beta\\
&\quad -\frac{-i}{4\pi^2}\int_0^{2\pi}\frac{v(\alpha)}{2}e^{-ik_1\alpha}d\alpha\int_0^{2\pi}e^{-i(k_2+d)\beta}d\beta\\
&= \frac{-i\hat{v}}{2}\delta(k_2-d) - \frac{-i\hat{v}}{2}\delta(k_2+d),\\
\hat{H}_\beta(v(\alpha)\sin(d\beta)) &= \frac{k_2}{\sqrt{k_1^2+k_2^2}}\left(-\frac{\hat{v}}{2}\delta(k_2-d)+\frac{\hat{v}}{2}\delta(k_2+d)\right)\\
&= \frac{-d}{\sqrt{k_1^2+d^2}}\frac{\hat{v}}{2}\delta(k_2-d)+\frac{-d}{\sqrt{k_1^2+d^2}}\frac{\hat{v}}{2}\delta(k_2+d)\\
&= \frac{-d}{\sqrt{k_1^2+d^2}}\hat{v}\left(\frac{\delta(k_2-d)}{2}+\frac{\delta(k_2+d)}{2}\right),\\
H_\beta(v(\alpha)\sin(d\beta)) &= \widetilde{\left(\frac{-d}{\sqrt{k_1^2+d^2}}\hat{v}\right)}\cos(d\beta)
\end{aligned}
$$

Therefore the following three operators will be used in this model, enabling the method to proceed without requiring β, and with the last two illustrating d dependence:

$$H_\alpha(v(\alpha)) = (-i\ \widetilde{\operatorname{sign}(k_1)}\,\hat{v}) \tag{38}$$

$$H_\alpha(v(\alpha)\cos(d\beta)) = \widetilde{\left(\frac{-ik_1}{\sqrt{k_1^2+d^2}}\hat{v}\right)}\cos(d\beta) \tag{39}$$

$$H_\beta(v(\alpha)\sin(d\beta)) = \widetilde{\left(\frac{-d}{\sqrt{k_1^2+d^2}}\hat{v}\right)}\cos(d\beta) \tag{40}$$

V. Linearization of Small-Scale Vortex Sheet Model

For the vortex sheet model, periodic waves of a traveling (in the x-direction) wave solution, $(x(\alpha), \sigma\beta, z(\alpha))$, are homogeneous in the β direction with trivial y dependence, where σ is dependent on the arc length of the one-dimensional interface. In order to preserve the isothermal parameterization of Equations (26)-(27), $\sigma^2 = x_a^2 + z_a^2$. The solver seeks functions that observe the following parities, Figure 12, where $\tilde{x} = x - \alpha$ and $\tilde{y} = y - \sigma\beta$ are periodic in order to effectively use the Fast Fourier Transform in the function approximation.

	Coordinate	
	α	β
$\tilde{x}(\alpha, \beta)$	odd	even
$\tilde{y}(\alpha, \beta)$	even	odd
$z(\alpha, \beta)$	even	even
$\mu(\alpha, \beta)$	odd	even

Figure 12. Function parities sought in the vortex sheet formulation.

The following weakly three-dimensional linearization ansatz is proposed, $\varepsilon \ll 1$, using an $O(\varepsilon)$ perturbation to the planar traveling wave solution informed by the parities of Figure 12:

$$\begin{aligned} x(\alpha, \beta) &= x_0(\alpha) + \varepsilon x_1(\alpha)\cos(d\beta) \\ y(\alpha, \beta) &= \sigma\beta + \varepsilon y_1(\alpha)\sin(d\beta) \\ z(\alpha, \beta) &= z_0(\alpha) + \varepsilon z_1(\alpha)\cos(d\beta) \\ \mu(\alpha, \beta) &= \mu_0(\alpha) + \varepsilon \mu_1(\alpha)\cos(d\beta) \end{aligned} \tag{41}$$

In addition to the matching parities, all of the perturbation functions, subscripted by 1, have zero mean. Any mean in the x and y parameterizations of α, β would indicate a shift of coordinates and can be ignored. The depth of each domain above and below the free-surface of the interfacial flow, z, is infinite and is therefore invariant

to shift. The mean of μ is the mean vortex sheet strength, which is an input parameter that we set to zero. These will be enforced in the quasi-Newton solver.

It was unclear whether the speed, c, and length, σ, terms required an $O(\varepsilon)$ adjustment in the linearization. Both terms were evaluated using the full small-scale approximation model at several small-amplitude planar waves. The bifurcation periods of these tests were found by a guess-and-check method. This was done to ensure that the linearization ansatz was correct. Log-log plots of σ and c versus ε for one amplitude of $h = 0.8229$ follow.

The general linearization of the speed is $c = c_0 + \varepsilon c_1 + \varepsilon^2 c_2 + O(\varepsilon^3)$. After subtracting c_0 from the planar bifurcation, $\Delta c = \varepsilon c_1 + \varepsilon^2 c_2 + O(\varepsilon^3)$. In the log-log plot of Figure 13, the remaining variation is seen to be $O(\varepsilon^2)$. Therefore, c_1 does not need to be included in the ansatz. The same is true for σ_1 (see Figure 14).

The following sections detail the linearization of the vortex sheet system, equations (24) - (27). Each $O(\varepsilon)$ piece is used in the dimension-breaking numerical code in order to find the appropriate bifurcation period.

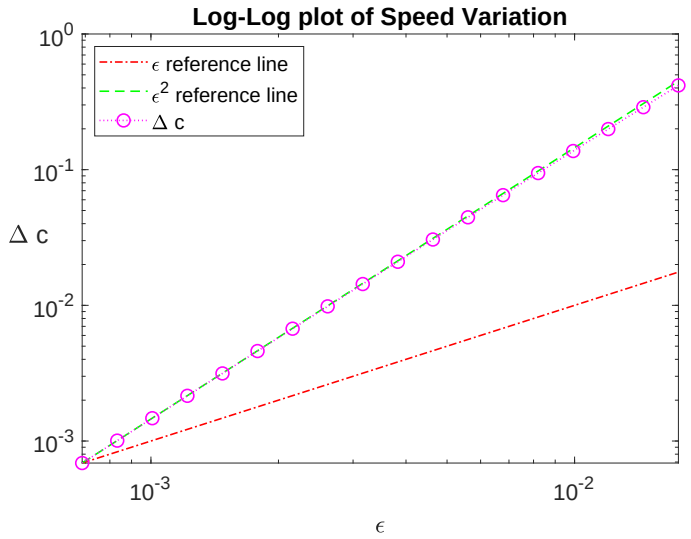

Figure 13. Log-Log plot of difference of speed, c in fully 3-D wave from the planar wave in the vortex sheet formulation, equations (24)-(27).

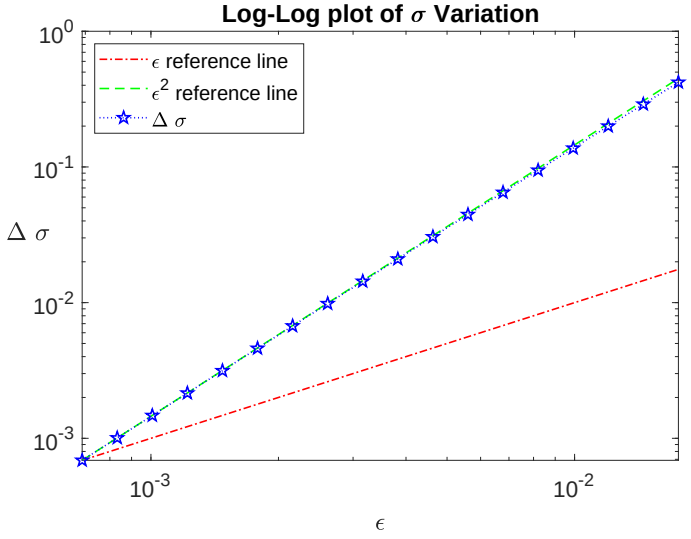

Figure 14. Log-Log plot of difference of arc length, σ, in fully 3-D wave from the planar wave in the vortex sheet formulation, equations (24)-(27).

5.1 Fundamental Forms and Taylor Expansions

Throughout the model equations (24)-(27), there are instances of E, G in the denominators of terms. In order to effectively use the $O(1)$ and $O(\varepsilon)$ parts, they will require Taylor expansions about the one-dimensional interface parameterized functions, f_0.

$$\begin{aligned} E =& X_\alpha \cdot X_\alpha = \begin{pmatrix} x_\alpha \\ y_\alpha \\ z_\alpha \end{pmatrix} \cdot \begin{pmatrix} x_\alpha \\ y_\alpha \\ z_\alpha \end{pmatrix} = x_\alpha^2 + y_\alpha^2 + z_\alpha^2 \\ =& \left(x_{0,\alpha}^2 + z_{0,\alpha}^2\right) + \varepsilon 2 \left(x_{0,\alpha} x_{1,\alpha} + z_{0,\alpha} z_{1,\alpha}\right) \cos(d\beta) + O(\varepsilon^2) \\ =& A + \varepsilon B + O(\varepsilon^2) \end{aligned}$$

In which,

$$A = \left(x_{0,\alpha}^2 + z_{0,\alpha}^2\right) = \sigma^2, B = 2 \left(x_{0,\alpha} x_{1,\alpha} + z_{0,\alpha} z_{1,\alpha}\right) \cos(d\beta) \tag{42}$$

The Taylor expansion of the form $\frac{1}{(A+\varepsilon B)^p} = A^{-p} - pA^{-p-1}B\varepsilon + O(\varepsilon^2)$, and the following forms appear in the vortex sheet formulation (24)-(27):

$$\begin{aligned} \frac{1}{E^{1/2}} &= A^{-1/2} - \frac{1}{2} A^{-3/2} B\varepsilon + O(\varepsilon^2) \\ \frac{1}{E} &= A^{-1} - A^{-2} B\varepsilon + O(\varepsilon^2) \\ \frac{1}{E^{3/2}} &= A^{-3/2} - \frac{3}{2} A^{-5/2} B\varepsilon + O(\varepsilon^2) \end{aligned} \tag{43}$$

Combining Equations (42) and (43) gives

$$\begin{aligned}
\frac{1}{E^{1/2}} &= \frac{1}{\sigma} - \varepsilon \left(\frac{(x_{0,\alpha} x_{1,\alpha} + z_{0,\alpha} z_{1,\alpha})}{\sigma^3} \right) \cos(d\beta) + O(\varepsilon^2) \\
\frac{1}{E} &= \frac{1}{\sigma^2} - \varepsilon \left(\frac{2\,(x_{0,\alpha} x_{1,\alpha} + z_{0,\alpha} z_{1,\alpha})}{\sigma^4} \right) \cos(d\beta) + O(\varepsilon^2) \\
\frac{1}{E^{3/2}} &= \frac{1}{\sigma^3} - \varepsilon \left(3\frac{(x_{0,\alpha} x_{1,\alpha} + z_{0,\alpha} z_{1,\alpha})}{\sigma^5} \right) \cos(d\beta) + O(\varepsilon^2)
\end{aligned}$$

Likewise, we can linearize the second fundamental form, G,

$$\begin{aligned}
G =& X_\beta \cdot X_\beta = \begin{pmatrix} x_\beta \\ y_\beta \\ z_\beta \end{pmatrix} \cdot \begin{pmatrix} x_\beta \\ y_\beta \\ z_\beta \end{pmatrix} = x_\beta^2 + y_\beta^2 + z_\beta^2 \\
=& \sigma^2 + \varepsilon 2\,(\sigma y_1 d)\cos(d\beta) + O(\varepsilon^2) \\
\frac{1}{G^{1/2}} =& \frac{1}{\sigma} - \varepsilon \frac{1}{\sigma^2}\,(y_1 d)\cos(d\beta) + O(\varepsilon^2)
\end{aligned}$$

These Taylor expansions of the fundamental forms E and G are now in a useful $O(1) + O(\varepsilon)$ format. This will allow them to be used more easily in the remaining pieces of the linearization.

5.2 Small-Scale Birkhoff-Rott Approximation

In the formulation used by Akers and Reeger [26], the small-scale approximation to the Birkhoff-Rott integral is:

$$W \approx H_\alpha \left[-\frac{\mu_\alpha X_\beta \times X_\alpha}{2E^{3/2}} \right] - H_\beta \left[-\frac{\mu_\beta X_\alpha \times X_\beta}{2E^{3/2}} \right]$$

where the H terms are Reisz Transformations. Note that this formulation depends on the assumption $\lambda = 1$ (both terms being divided by E instead of one by G). Given

that $X_\alpha \times X_\beta = -X_\beta \times X_\alpha$,

$$W \approx \frac{1}{2}\left(H_\alpha\left[-\frac{\mu_\alpha X_\beta \times X_\alpha}{E^{3/2}}\right] + H_\beta\left[-\frac{\mu_\beta X_\beta \times X_\alpha}{E^{3/2}}\right]\right)$$

In order to linearize W, note that a large portion of the two terms under the Reisz transformations are the same. Beginning with the cross product,

$$X_\beta \times X_\alpha = \begin{pmatrix} y_\beta z_\alpha - z_\beta y_\alpha \\ z_\beta x_\alpha - x_\beta z_\alpha \\ x_\beta y_\alpha - y_\beta x_\alpha \end{pmatrix} = \begin{pmatrix} \sigma z_{0,\alpha} \\ 0 \\ -\sigma x_{0,\alpha} \end{pmatrix} + \varepsilon \begin{pmatrix} [\sigma z_{1,\alpha} + y_1 z_{0,\alpha} d]\cos(d\beta) \\ [x_1 z_{0,\alpha} - x_{0,\alpha} z_1]\, d\sin(d\beta) \\ [-\sigma x_{1,\alpha} - x_{0,\alpha} y_1 d]\cos(d\beta) \end{pmatrix} + O(\varepsilon^2)$$

and including the Taylor expansion:

$$\frac{1}{E^{3/2}} = \frac{1}{\sigma^3} - \varepsilon\left(\frac{3\left(x_{0,\alpha}x_{1,\alpha} + z_{0,\alpha}z_{1,\alpha}\right)}{\sigma^5}\right)\cos(d\beta) + O(\varepsilon^2)$$

gives

$$\begin{aligned} \frac{X_\beta \times X_\alpha}{E^{3/2}} = {} & \frac{1}{\sigma^2}\begin{pmatrix} z_{0,\alpha} \\ 0 \\ -x_{0,\alpha} \end{pmatrix} \\ & + \varepsilon\left[\frac{1}{\sigma^4}\begin{pmatrix} (\sigma^2 z_{1,\alpha} + \sigma y_1 z_{0,\alpha} d - 3z_{0,\alpha}\left(x_{0,\alpha}x_{1,\alpha} + z_{0,\alpha}z_{1,\alpha}\right))\cos(d\beta) \\ \sigma\left[x_1 z_{0,\alpha} - x_{0,\alpha} z_1\right] d\sin(d\beta) \\ (-\sigma^2 x_{1,\alpha} - \sigma x_{0,\alpha} y_1 d + 3x_{0,\alpha}\left(x_{0,\alpha}x_{1,\alpha} + z_{0,\alpha}z_{1,\alpha}\right))\cos(d\beta) \end{pmatrix}\right] \\ & + O(\varepsilon^2) \end{aligned} \tag{44}$$

Equation (44) is multiplied by either μ_α or μ_β in the small-scale approximation. Both

terms are presented below:

$$\begin{aligned}\mu_\alpha \frac{X_\beta \times X_\alpha}{E^{3/2}} =& \frac{1}{\sigma^2}\begin{pmatrix} z_{0,\alpha}\mu_{0,\alpha} \\ 0 \\ -x_{0,\alpha}\mu_{0,\alpha} \end{pmatrix} \\ &+ \varepsilon \left[\frac{1}{\sigma^4} \begin{pmatrix} \left(\sigma^2 z_{1,\alpha} + \sigma y_1 z_{0,\alpha} d - 3z_{0,\alpha}\left(x_{0,\alpha}x_{1,\alpha} + z_{0,\alpha}z_{1,\alpha}\right)\right)\mu_{0,\alpha}\cos(d\beta) \\ \sigma\left[x_1 z_{0,\alpha} - x_{0,\alpha}z_1\right] d\mu_{0,\alpha}\sin(d\beta) \\ \left(-\sigma^2 x_{1,\alpha} - \sigma x_{0,\alpha} y_1 d + 3x_{0,\alpha}\left(x_{0,\alpha}x_{1,\alpha} + z_{0,\alpha}z_{1,\alpha}\right)\right)\mu_{0,\alpha}\cos(d\beta) \end{pmatrix} \right. \\ &\left. + \frac{1}{\sigma^2}\begin{pmatrix} z_{0,\alpha}\mu_{1,\alpha}\cos(d\beta) \\ 0 \\ -x_{0,\alpha}\mu_{1,\alpha}\cos(d\beta) \end{pmatrix} \right] + O(\varepsilon^2), \end{aligned} \tag{45}$$

$$\mu_\beta \frac{X_\beta \times X_\alpha}{E^{3/2}} = \varepsilon \frac{d}{\sigma^2}\begin{pmatrix} -z_{0,\alpha}\mu_1 \\ 0 \\ x_{0,\alpha}\mu_1 \end{pmatrix}\sin(d\beta) + O(\varepsilon^2) \tag{46}$$

Together (45) and (46) are produce the following small-scale linearization of W.

$$\begin{aligned} W \approx& \frac{1}{2}H_\alpha \left[\frac{1}{\sigma^3}\begin{pmatrix} -z_{0,\alpha}\mu_{0,\alpha} \\ 0 \\ x_{0,\alpha}\mu_{0,\alpha} \end{pmatrix} \right] \\ &+ \varepsilon\frac{1}{2}\left(H_\alpha \left[\frac{1}{\sigma^5} \begin{pmatrix} -\mu_{0,\alpha}\left(\sigma^2\left[z_{1,\alpha} + y_1 z_{0,\alpha} d\right] - 3z_{0,\alpha}\left(x_{0,\alpha}x_{1,\alpha} + z_{0,\alpha}z_{1,\alpha}\right)\right)\cos(d\beta) \\ -\mu_{0,\alpha}\sigma^2\left[x_1 z_{0,\alpha} - x_{0,\alpha}z_1\right] d\sin(d\beta) \\ -\mu_{0,\alpha}\left(\sigma^2\left[-x_{1,\alpha} - x_{0,\alpha}y_1 d\right] + 3x_{0,\alpha}\left(x_{0,\alpha}x_{1,\alpha} + z_{0,\alpha}z_{1,\alpha}\right)\right)\cos(d\beta) \end{pmatrix} \right. \right. \\ &\left. \left. + \frac{1}{\sigma^3}\begin{pmatrix} -z_{0,\alpha}\mu_{1,\alpha}\cos(d\beta) \\ 0 \\ x_{0,\alpha}\mu_{1,\alpha}\cos(d\beta) \end{pmatrix} \right] + H_\beta \left[\frac{d}{\sigma^3}\begin{pmatrix} -z_{0,\alpha}\mu_1 \\ 0 \\ x_{0,\alpha}\mu_1 \end{pmatrix}\sin(d\beta) \right] \right) + O(\varepsilon^2) \end{aligned}$$

For use in the linearization ansatz (41), we also denote the following terms, where the superscript indicates the entry of a vector:

$$W_0 = \begin{pmatrix} W_0^{(1)} \\ W_0^{(2)} \\ W_0^{(3)} \end{pmatrix}, W_1 = \begin{pmatrix} W_1^{(1)} \\ W_1^{(2)} \\ W_1^{(3)} \end{pmatrix}, D(\beta) = \begin{pmatrix} \cos(d\beta) & 0 & 0 \\ 0 & \sin(d\beta) & 0 \\ 0 & 0 & \cos(d\beta) \end{pmatrix}$$

so that

$$W = W_0 + \varepsilon D(\beta) W_1 + O(\varepsilon^2)$$

Keeping the $O(1)$ and $O(\varepsilon)$ pieces of the velocity expansion isolated in these terms will allow an easy switch from approximations to the full Birkhoff-Rott integral in future work.

Therefore, in the Small-Scale Approximation and under the assumption $d > 0$:

$$\begin{aligned}
W_0^{(1)} =& \frac{1}{2} H_\alpha \left[\frac{-z_{0,\alpha}\mu_{0,\alpha}}{\sigma^3} \right] \\
W_0^{(2)} =& 0 \\
W_0^{(3)} =& \frac{1}{2} H_\alpha \left[\frac{x_{0,\alpha}\mu_{0,\alpha}}{\sigma^3} \right] \\
W_1^{(1)} =& A_1^{(1)} + B_1^{(1)} \\
& A_1^{(1)} = \frac{1}{2} H_\alpha \left[\frac{3}{\sigma^5} \mu_{0,\alpha} z_{0,\alpha} \left(x_{0,\alpha} x_{1,\alpha} + z_{0,\alpha} z_{1,\alpha} \right) \right. \\
& \qquad \left. + \frac{1}{\sigma^3} \left(-z_{0,\alpha}\mu_{1,\alpha} - \mu_{0,\alpha} z_{1,\alpha} - \mu_{0,\alpha} z_{0,\alpha} \left(x_{0,\alpha} x_{1,\alpha} + z_{0,\alpha} z_{1,\alpha} \right) \right) \right] \\
& B_1^{(1)} = -\frac{1}{2} H_\beta \left[\frac{d}{\sigma^3} z_{0,\alpha} \mu_1 \right] \\
W_1^{(2)} =& \frac{1}{2} H_\alpha \left[\frac{d}{\sigma^3} \mu_{0,\alpha} \left(x_{0,\alpha} z_1 - x_1 z_{0,\alpha} \right) \sin(d\beta) \right]
\end{aligned}$$

$$
\begin{aligned}
W_1^{(3)} =& A_1^{(3)} + B_1^{(3)} \\
& A_1^{(3)} = \frac{1}{2} H_\alpha \left[\frac{-3}{\sigma^5} \mu_{0,\alpha} x_{0,\alpha} \left(x_{0,\alpha} x_{1,\alpha} + z_{0,\alpha} z_{1,\alpha} \right) \right. \\
& \qquad \left. + \frac{1}{\sigma^3} \left(\mu_{0,\alpha} x_{1,\alpha} + \mu_{0,\alpha} x_{0,\alpha} \left(x_{0,\alpha} x_{1,\alpha} + z_{0,\alpha} z_{1,\alpha} \right) + x_{0,\alpha} \mu_{1,\alpha} \right) \right] \\
& B_1^{(3)} = \frac{1}{2} H_\beta \left[\frac{d}{\sigma^3} x_{0,\alpha} \mu_1 \right]
\end{aligned}
$$

5.3 Isothermal Parameterization

The last two equations of the vortex sheet model, equations (26)-(27), are the isothermal parameterization equations. These equations are the two-dimensional surface analog of the arc length parameterization used in the one-dimensional interface. Equation (26) locally enforces right angles between the α and β parameterizations, and equation (27) is an aspect ratio of the parameterization of α and β. They are linearized in the following subsections.

Perpendicular Equation

The perpendicular (23) equation is:

$$
0 = \begin{pmatrix} x_\alpha \\ y_\alpha \\ z_\alpha \end{pmatrix} \cdot \begin{pmatrix} x_\beta \\ y_\beta \\ z_\beta \end{pmatrix}
$$

Using the ansatz equations (41), we have:

$$
\begin{aligned}
0 =& \begin{pmatrix} x_{0,\alpha} + \varepsilon x_{1,\alpha} \cos(d\beta) \\ \varepsilon y_{1,\alpha} \sin(d\beta) \\ z_{0,\alpha} + \varepsilon z_{1,\alpha} \cos(d\beta) \end{pmatrix} \cdot \begin{pmatrix} -\varepsilon x_1 d \sin(d\beta) \\ \sigma + \varepsilon y_1 d \cos(d\beta) \\ -\varepsilon z_1 d \sin(d\beta) \end{pmatrix} \\
0 =& \varepsilon \left(-x_{0,\alpha} x_1 d + \sigma y_{1,\alpha} - z_{0,\alpha} z_1 d \right) \sin(d\beta) + O(\varepsilon^2)
\end{aligned}
$$

So that at $O(\varepsilon)$,

$$0 = -x_{0,\alpha}x_1 d + \sigma y_{1,\alpha} - z_{0,\alpha}z_1 d \tag{47}$$

Aspect Equation

The aspect equation (24) is:

$$\lambda G = E$$

$$\lambda \begin{pmatrix} x_\beta \\ y_\beta \\ z_\beta \end{pmatrix} \cdot \begin{pmatrix} x_\beta \\ y_\beta \\ z_\beta \end{pmatrix} = \begin{pmatrix} x_\alpha \\ y_\alpha \\ z_\alpha \end{pmatrix} \cdot \begin{pmatrix} x_\alpha \\ y_\alpha \\ z_\alpha \end{pmatrix}$$

Using the ansatz equation (41), we have:

$$\lambda \begin{pmatrix} & -\varepsilon x_1 d\sin(d\beta) \\ \sigma & +\varepsilon y_1 d\cos(d\beta) \\ & -\varepsilon z_1 d\sin(d\beta) \end{pmatrix} \cdot \begin{pmatrix} & -\varepsilon x_1 d\sin(d\beta) \\ \sigma & +\varepsilon y_1 d\cos(d\beta) \\ & -\varepsilon z_1 d\sin(d\beta) \end{pmatrix} =$$

$$\begin{pmatrix} x_{0,\alpha} + \varepsilon x_{1,\alpha}\cos(d\beta) \\ \varepsilon y_{1,\alpha}\sin(d\beta) \\ z_{0,\alpha} + \varepsilon z_{1,\alpha}\cos(d\beta) \end{pmatrix} \cdot \begin{pmatrix} x_{0,\alpha} + \varepsilon x_{1,\alpha}\cos(d\beta) \\ \varepsilon y_{1,\alpha}\sin(d\beta) \\ z_{0,\alpha} + \varepsilon z_{1,\alpha}\cos(d\beta) \end{pmatrix}$$

$$\lambda\sigma^2 + \varepsilon\left(2\sigma y_1 d\right)\lambda\cos(d\beta) + O(\varepsilon^2) = \left(x_{0,\alpha}^2 + z_{0,\alpha}^2\right) + \varepsilon 2\left(x_{0,\alpha}x_{1,\alpha} + z_{0,\alpha}z_{1,\alpha}\right)\cos(d\beta) + O(\varepsilon^2)$$

At $O(\varepsilon)$, this gives:

$$0 = x_{0,\alpha}x_{1,\alpha} + z_{0,\alpha}z_{1,\alpha} - \lambda\sigma y_1 d \tag{48}$$

5.4 Tangent and Normal Vectors

In the α, β parameterization, the unit tangent and normal vectors are:

$$\begin{aligned}
\boldsymbol{t}_1 =& \frac{X_\alpha}{||X_\alpha||} = X_\alpha \frac{1}{E^{1/2}} \\
\boldsymbol{t}_2 =& \frac{X_\beta}{||X_\beta||} = X_\beta \frac{1}{G^{1/2}} \\
\boldsymbol{n} =& \boldsymbol{t}_1 \times \boldsymbol{t}_2
\end{aligned}$$

In this linearization with ansatz equations (41):

$$\begin{aligned}
\boldsymbol{t}_1 =& \begin{pmatrix} x_{0,\alpha} + \varepsilon x_{1,\alpha}\cos(d\beta) \\ \varepsilon y_{1,\alpha}\sin(d\beta) \\ z_{0,\alpha} + \varepsilon z_{1,\alpha}\cos(d\beta) \end{pmatrix} \left(\frac{1}{\sigma} - \varepsilon \left(\frac{(x_{0,\alpha}x_{1,\alpha} + z_{0,\alpha}z_{1,\alpha})}{\sigma^3} \right) \cos(d\beta) + O(\varepsilon^2) \right) \\
=& \frac{1}{\sigma} \begin{pmatrix} x_{0,\alpha} \\ 0 \\ z_{0,\alpha} \end{pmatrix} + \varepsilon \frac{1}{\sigma} \begin{pmatrix} \left[x_{1,\alpha} - \frac{1}{\sigma^2} \left(x_{0,\alpha}^2 x_{1,\alpha} + z_{0,\alpha}z_{1,\alpha}x_{0,\alpha} \right) \right] \cos(d\beta) \\ y_{1,\alpha}\sin(d\beta) \\ \left[z_{1,\alpha} - \frac{1}{\sigma^2} \left(z_{0,\alpha}x_{0,\alpha}x_{1,\alpha} + z_{0,\alpha}^2 z_{1,\alpha} \right) \right] \cos(d\beta) \end{pmatrix} + O(\varepsilon^2) \\
=& \frac{1}{\sigma} \begin{pmatrix} x_{0,\alpha} \\ 0 \\ z_{0,\alpha} \end{pmatrix} + \varepsilon \frac{1}{\sigma^3} \begin{pmatrix} \left[z_{0,\alpha} \left(z_{0,\alpha}x_{1,\alpha} - z_{1,\alpha}x_{0,\alpha} \right) \right] \cos(d\beta) \\ \sigma^2 y_{1,\alpha}\sin(d\beta) \\ \left[x_{0,\alpha} \left(-z_{0,\alpha}x_{1,\alpha} + x_{0,\alpha}z_{1,\alpha} \right) \right] \cos(d\beta) \end{pmatrix} + O(\varepsilon^2)
\end{aligned} \tag{49}$$

$$\begin{aligned}
\boldsymbol{t}_2 =& \begin{pmatrix} -\varepsilon x_1 d\sin(d\beta) \\ \sigma + \varepsilon y_1 d\cos(d\beta) \\ -\varepsilon z_1 d\sin(d\beta) \end{pmatrix} \left(\frac{1}{\sigma} - \varepsilon \frac{1}{\sigma^2} \left(y_1 d \right) \cos(d\beta) + O(\varepsilon^2) \right) \\
=& \begin{pmatrix} 0 \\ 1 \\ 0 \end{pmatrix} - \varepsilon \frac{d}{\sigma} \begin{pmatrix} x_1 \sin(d\beta) \\ 0 \\ z_1 \sin(d\beta) \end{pmatrix} + O(\varepsilon^2)
\end{aligned} \tag{50}$$

For the normal vector, recall:

$$\begin{aligned}
\boldsymbol{n} =& \boldsymbol{t}_1 \times \boldsymbol{t}_2 \\
\boldsymbol{n}^{(1)} =& \boldsymbol{t}_1^{(2)} \boldsymbol{t}_2^{(3)} - \boldsymbol{t}_1^{(3)} \boldsymbol{t}_2^{(2)} \\
\boldsymbol{n}^{(2)} =& \boldsymbol{t}_1^{(3)} \boldsymbol{t}_2^{(1)} - \boldsymbol{t}_1^{(1)} \boldsymbol{t}_2^{(3)} \\
\boldsymbol{n}^{(3)} =& \boldsymbol{t}_1^{(1)} \boldsymbol{t}_2^{(2)} - \boldsymbol{t}_1^{(2)} \boldsymbol{t}_2^{(1)}
\end{aligned}$$

therefore after using the linearized versions of the tangent equations, the normal vector is as follows:

$$\begin{aligned}
\boldsymbol{n}^{(1)} =& \left(\varepsilon \frac{1}{\sigma} y_{1,\alpha} \sin(d\beta) + O(\varepsilon^2) \right) \left(-\varepsilon d z_1 \sin(d\beta) + O(\varepsilon^2) \right) \\
& - \left(\frac{1}{\sigma} z_{0,\alpha} + \varepsilon \frac{1}{\sigma^3} \left[x_{0,\alpha} \left(-z_{0,\alpha} x_{1,\alpha} + x_{0,\alpha} z_{1,\alpha} \right) \right] \cos(d\beta) + O(\varepsilon^2) \right) \left(1 + O(\varepsilon^2) \right) \\
=& -\frac{1}{\sigma} z_{0,\alpha} - \varepsilon \frac{1}{\sigma^3} \left[x_{0,\alpha} \left(-z_{0,\alpha} x_{1,\alpha} + x_{0,\alpha} z_{1,\alpha} \right) \right] \cos(d\beta) + O(\varepsilon^2)
\end{aligned} \tag{51}$$

$$\begin{aligned}
\boldsymbol{n}^{(2)} =& \left(\frac{1}{\sigma} z_{0,\alpha} + O(\varepsilon) \right) \left(-\varepsilon \frac{d}{\sigma} x_1 \sin(d\beta) + O(\varepsilon^2) \right) \\
& - \left(\frac{1}{\sigma} x_{0,\alpha} + O(\varepsilon) \right) \left(-\varepsilon \frac{d}{\sigma} z_1 \sin(d\beta) + O(\varepsilon^2) \right) \\
=& \varepsilon \frac{d}{\sigma^2} \left(x_{0,\alpha} z_1 - z_{0,\alpha} x_1 \right) \sin(d\beta) + O(\varepsilon^2)
\end{aligned} \tag{52}$$

$$\begin{aligned}
\boldsymbol{n}^{(3)} =& \left(\frac{1}{\sigma} x_{0,\alpha} + \varepsilon \frac{1}{\sigma^3} \left[z_{0,\alpha} \left(z_{0,\alpha} x_{1,\alpha} - z_{1,\alpha} x_{0,\alpha} \right) \right] \cos(d\beta) + O(\varepsilon^2) \right) \left(1 + O(\varepsilon^2) \right) \\
& - \left(\varepsilon \frac{1}{\sigma^3} \lambda \sigma^2 y_{1,\alpha} \sin(d\beta) + O(\varepsilon^2) \right) \left(-\varepsilon d x_1 \sin(d\beta) + O(\varepsilon^2) \right) \\
=& \frac{1}{\sigma} x_{0,\alpha} + \varepsilon \frac{1}{\sigma^3} \left[z_{0,\alpha} \left(z_{0,\alpha} x_{1,\alpha} - z_{1,\alpha} x_{0,\alpha} \right) \right] \cos(d\beta) + O(\varepsilon^2)
\end{aligned} \tag{53}$$

5.5 Kinematic Equation

All of the terms required for the kinematic equation (25) are now available and it can be linearized as follows:

$$
\begin{aligned}
0 =& c(\boldsymbol{n})_1 - W \cdot \boldsymbol{n} \\
=& -\frac{c}{\sigma} z_{0,\alpha} - \varepsilon \frac{c}{\sigma^3} \left[x_{0,\alpha} \left(-z_{0,\alpha} x_{1,\alpha} + x_{0,\alpha} z_{1,\alpha} \right) \right] \cos(d\beta) \\
& - \Bigg[\left(W_0^{(1)} + \varepsilon D_{1,1} W_1^{(1)} \right) \left(-\frac{1}{\sigma} z_{0,\alpha} - \varepsilon \frac{1}{\sigma^3} \left[x_{0,\alpha} \left(-z_{0,\alpha} x_{1,\alpha} + x_{0,\alpha} z_{1,\alpha} \right) \right] \cos(d\beta) + O(\varepsilon^2) \right) \\
& \quad + \left(W_0^{(2)} + \varepsilon D_{2,2} W_1^{(2)} \right) \left(\varepsilon \frac{d}{\sigma} \left(x_{0,\alpha} z_1 - z_{0,\alpha} x_1 \right) \sin(d\beta) + O(\varepsilon^2) \right) \\
& \quad + \left(W_0^{(3)} + \varepsilon D_{3,3} W_1^{(3)} \right) \left(\frac{1}{\sigma} x_{0,\alpha} + \varepsilon \frac{1}{\sigma^3} \left[z_{0,\alpha} \left(z_{0,\alpha} x_{1,\alpha} - z_{1,\alpha} x_{0,\alpha} \right) \right] \cos(d\beta) + O(\varepsilon^2) \right) \Bigg] \\
=& \frac{1}{\sigma} \left(W_0^{(1)} z_{0,\alpha} - W_0^{(3)} x_{0,\alpha} - c z_{0,\alpha} \right) \\
& + \varepsilon \frac{1}{\sigma^3} \Big(W_0^{(1)} \left[x_{0,\alpha} \left(-z_{0,\alpha} x_{1,\alpha} + x_{0,\alpha} z_{1,\alpha} \right) \right] \cos(d\beta) - W_0^{(2)} d\sigma^2 \left(x_{0,\alpha} z_1 - z_{0,\alpha} x_1 \right) \sin(d\beta) \\
& \quad - W_0^{(3)} \left[z_{0,\alpha} \left(z_{0,\alpha} x_{1,\alpha} - z_{1,\alpha} x_{0,\alpha} \right) \right] \cos(d\beta) - c \left[x_{0,\alpha} \left(-z_{0,\alpha} x_{1,\alpha} + x_{0,\alpha} z_{1,\alpha} \right) \right] \cos(d\beta) \\
& \quad + D_{1,1} W_1^{(1)} \sigma^2 z_{0,\alpha} - D_{3,3} W_1^{(3)} \sigma^2 x_{0,\alpha} \Big) \\
& + O(\varepsilon^2)
\end{aligned}
$$

In the small-scale approximation, $W_0^{(2)} = 0$, which allows the cosine function to be factored out:

$$
\begin{aligned}
0 =& c(\boldsymbol{n})_1 - W \cdot \boldsymbol{n} \\
=& \frac{1}{\sigma} \left(W_0^{(1)} z_{0,\alpha} - W_0^{(3)} x_{0,\alpha} - c z_{0,\alpha} \right) + \varepsilon \frac{1}{\sigma^3} \Bigg(W_0^{(1)} \left[x_{0,\alpha} \left(-z_{0,\alpha} x_{1,\alpha} + x_{0,\alpha} z_{1,\alpha} \right) \right] \\
& \quad + W_1^{(1)} \sigma^2 z_{0,\alpha} - W_0^{(3)} \left[z_{0,\alpha} \left(z_{0,\alpha} x_{1,\alpha} - z_{1,\alpha} x_{0,\alpha} \right) \right] - W_1^{(3)} \sigma^2 x_{0,\alpha} \\
& \quad - c \left[x_{0,\alpha} \left(-z_{0,\alpha} x_{1,\alpha} + x_{0,\alpha} z_{1,\alpha} \right) \right] \Bigg) \cos(d\beta) + O(\varepsilon^2)
\end{aligned} \tag{54}
$$

And at $O(\varepsilon)$:

$$\begin{aligned}0 =& W_0^{(1)}\left[x_{0,\alpha}\left(-z_{0,\alpha}x_{1,\alpha}+x_{0,\alpha}z_{1,\alpha}\right)\right]+W_1^{(1)}\sigma^2 z_{0,\alpha}-W_0^{(3)}\left[z_{0,\alpha}\left(z_{0,\alpha}x_{1,\alpha}-z_{1,\alpha}x_{0,\alpha}\right)\right]\\ &-W_1^{(3)}\sigma^2 x_{0,\alpha}-c\left[x_{0,\alpha}\left(-z_{0,\alpha}x_{1,\alpha}+x_{0,\alpha}z_{1,\alpha}\right)\right]\end{aligned} \tag{55}$$

5.6 Bernoulli Equation

The linearization of the Bernoulli equation (24) is challenging due to the number of terms. Looking for the $O(\varepsilon)$ piece of each additive term allows them to be isolated and handled separately. This is much more manageable. We begin with the curvature, which is not used elsewhere, and the tangential velocity terms, which factor into many of the remaining terms. From there, we will use the tangential velocity terms to linearize the remaining additive terms into their $O(1)$ and $O(\varepsilon)$ pieces.

Curvature

τ is the surface tension constant coupled with the curvature, $\kappa = \frac{L+\lambda N}{2E}$. E is as previously calculated and $L = X_{\alpha,\alpha}\cdot\boldsymbol{n}$, $N = X_{\beta,\beta}\cdot\boldsymbol{n}$.

$$\begin{aligned}L =& x_{\alpha,\alpha}\boldsymbol{n}^{(1)}+y_{\alpha,\alpha}\boldsymbol{n}^{(2)}+z_{\alpha,\alpha}\boldsymbol{n}^{(3)}\\ =&\left(x_{0,\alpha,\alpha}+\varepsilon x_{1,\alpha,\alpha}\cos(d\beta)\right)\left(-\frac{1}{\sigma}z_{0,\alpha}-\varepsilon\frac{1}{\sigma^3}\left[x_{0,\alpha}\left(-z_{0,\alpha}x_{1,\alpha}+x_{0,\alpha}z_{1,\alpha}\right)\right]\cos(d\beta)+O(\varepsilon^2)\right)\\ &+\left(\varepsilon y_{1,\alpha,\alpha}\sin(d\beta)\right)\left(\varepsilon\frac{d}{\sigma}\left(x_{0,\alpha}z_1-z_{0,\alpha}x_1\right)\sin(d\beta)+O(\varepsilon^2)\right)\\ &+\left(z_{0,\alpha,\alpha}+\varepsilon z_{1,\alpha,\alpha}\cos(d\beta)\right)\left(\frac{1}{\sigma}x_{0,\alpha}+\varepsilon\frac{1}{\sigma^3}\left[z_{0,\alpha}\left(z_{0,\alpha}x_{1,\alpha}-z_{1,\alpha}x_{0,\alpha}\right)\right]\cos(d\beta)+O(\varepsilon^2)\right)\\ =&\frac{1}{\sigma}\left(x_{0,\alpha}z_{0,\alpha,\alpha}-x_{0,\alpha,\alpha}z_{0,\alpha}\right)+\varepsilon\frac{1}{\sigma}\Bigg[\left(x_{0,\alpha}z_{1,\alpha,\alpha}-x_{1,\alpha,\alpha}z_{0,\alpha}\right)\\ &+\frac{1}{\sigma^2}\left(z_{0,\alpha,\alpha}z_{0,\alpha}\left(z_{0,\alpha}x_{1,\alpha}-z_{1,\alpha}x_{0,\alpha}\right)-x_{0,\alpha,\alpha}x_{0,\alpha}\left(-z_{0,\alpha}x_{1,\alpha}+x_{0,\alpha}z_{1,\alpha}\right)\right)\Bigg]\cos(d\beta)\end{aligned}$$

$$
\begin{aligned}
N =& x_{\beta,\beta}\boldsymbol{n}^{(1)} + y_{\beta,\beta}\boldsymbol{n}^{(2)} + z_{\beta,\beta}\boldsymbol{n}^{(3)} \\
&= \left(-\varepsilon x_1 d^2 \cos(d\beta)\right)\left(-\frac{1}{\sigma} z_{0,\alpha} - \varepsilon \frac{1}{\sigma^3}\left[x_{0,\alpha}\left(-z_{0,\alpha}x_{1,\alpha} + x_{0,\alpha}z_{1,\alpha}\right)\right]\cos(d\beta) + O(\varepsilon^2)\right) \\
&+ \left(-\varepsilon y_1 d^2 \sin(d\beta)\right)\left(\varepsilon \frac{d}{\sigma}\left(x_{0,\alpha}z_1 - z_{0,\alpha}x_1\right)\sin(d\beta) + O(\varepsilon^2)\right) \\
&+ \left(-\varepsilon z_1 d^2 \cos(d\beta)\right)\left(\frac{1}{\sigma} x_{0,\alpha} + \varepsilon \frac{1}{\sigma^3}\left[z_{0,\alpha}\left(z_{0,\alpha}x_{1,\alpha} - z_{1,\alpha}x_{0,\alpha}\right)\right]\cos(d\beta) + O(\varepsilon^2)\right) \\
=& \varepsilon \frac{d^2}{\sigma}\left(z_{0,\alpha}x_1 - x_{0,\alpha}z_1\right)\cos(d\beta)
\end{aligned}
$$

In the numerator of κ, this yields

$$
\begin{aligned}
L + \lambda N =& \frac{1}{\sigma}\left(x_{0,\alpha}z_{0,\alpha,\alpha} - x_{0,\alpha,\alpha}z_{0,\alpha}\right) \\
&+ \varepsilon\left(\frac{\lambda d^2}{\sigma}\left(z_{0,\alpha}x_1 - x_{0,\alpha}z_1\right) + \frac{1}{\sigma}\left(x_{0,\alpha}z_{1,\alpha,\alpha} - x_{1,\alpha,\alpha}z_{0,\alpha}\right)\right. \\
&\qquad \left. + \frac{1}{\sigma^3}\left(z_{0,\alpha,\alpha}z_{0,\alpha}\left(z_{0,\alpha}x_{1,\alpha} - z_{1,\alpha}x_{0,\alpha}\right) - x_{0,\alpha,\alpha}x_{0,\alpha}\left(-z_{0,\alpha}x_{1,\alpha} + x_{0,\alpha}z_{1,\alpha}\right)\right)\right)\cos(d\beta) \\
&+ O(\varepsilon^2)
\end{aligned}
$$

which will be multiplied by the E term,

$$
\frac{1}{2E} = \frac{1}{2\sigma^2} - \varepsilon\left(\frac{\left(x_{0,\alpha}x_{1,\alpha} + z_{0,\alpha}z_{1,\alpha}\right)}{\sigma^4}\right)\cos(d\beta) + O(\varepsilon^2)
$$

The fully linearized curvature term is therefore,

$$
\begin{aligned}
\kappa =& \frac{1}{2\sigma^3}\left(x_{0,\alpha}z_{0,\alpha,\alpha} - x_{0,\alpha,\alpha}z_{0,\alpha}\right) \\
&+ \varepsilon\left(\frac{\lambda d^2}{2\sigma^3}\left(z_{0,\alpha}x_1 - x_{0,\alpha}z_1\right) + \frac{1}{2\sigma^3}\left(x_{0,\alpha}z_{1,\alpha,\alpha} - x_{1,\alpha,\alpha}z_{0,\alpha}\right)\right. \\
&\quad + \frac{1}{2\sigma^5}\left(z_{0,\alpha,\alpha}z_{0,\alpha}\left(z_{0,\alpha}x_{1,\alpha} - z_{1,\alpha}x_{0,\alpha}\right) - x_{0,\alpha,\alpha}x_{0,\alpha}\left(-z_{0,\alpha}x_{1,\alpha} + x_{0,\alpha}z_{1,\alpha}\right)\right) \\
&\quad \left. - \frac{1}{\sigma^5}\left(x_{0,\alpha}z_{0,\alpha,\alpha} - x_{0,\alpha,\alpha}z_{0,\alpha}\right)\left(x_{0,\alpha}x_{1,\alpha} + z_{0,\alpha}z_{1,\alpha}\right)\right)\cos(d\beta) + O(\varepsilon^2)
\end{aligned}
$$

Tangential Velocity Terms

For the remaining pieces, we will need to linearize the tangential velocity of the fluid particles, $W \cdot \boldsymbol{t}_i$, and of the interface motion, $c\boldsymbol{t}_i^{(1)}$:

$$\begin{aligned}
W \cdot \boldsymbol{t}_1 = &\left[\left(W_0^{(1)} + \varepsilon D_{1,1} W_1^{(1)}\right)\left(\frac{1}{\sigma} x_{0,\alpha} + \varepsilon \frac{1}{\sigma^3}\left[z_{0,\alpha}\left(z_{0,\alpha}x_{1,\alpha} - z_{1,\alpha}x_{0,\alpha}\right)\right]\cos(d\beta) + O(\varepsilon^2)\right)\right. \\
&\quad + \left(W_{0,y} + \varepsilon D_{2,2} W_{1,y}\right)\left(\varepsilon \frac{1}{\sigma} y_{1,\alpha}\sin(d\beta) + O(\varepsilon^2)\right) \\
&\left. + \left(W_0^{(3)} + \varepsilon D_{3,3} W_1^{(3)}\right)\left(\frac{1}{\sigma} z_{0,\alpha} + \varepsilon \frac{1}{\sigma^3}\left[x_{0,\alpha}\left(-z_{0,\alpha}x_{1,\alpha} + x_{0,\alpha}z_{1,\alpha}\right)\right]\cos(d\beta) + O(\varepsilon^2)\right)\right] \\
= &\frac{1}{\sigma}\left(W_0^{(1)} x_{0,\alpha} + W_0^{(3)} z_{0,\alpha}\right) \\
&+ \varepsilon\left(\frac{1}{\sigma}\left(D_{1,1}W_1^{(1)}x_{0,\alpha} + D_{3,3}W_1^{(3)}z_{0,\alpha}\right) + W_{0,y}\frac{1}{\sigma}y_{1,\alpha}\sin(d\beta)\right. \\
&\quad \left. + \frac{1}{\sigma^3}\left(W_0^{(1)}\left[z_{0,\alpha}\left(z_{0,\alpha}x_{1,\alpha} - z_{1,\alpha}x_{0,\alpha}\right)\right] + W_0^{(3)}\left[x_{0,\alpha}\left(-z_{0,\alpha}x_{1,\alpha} + x_{0,\alpha}z_{1,\alpha}\right)\right]\right)\cos(d\beta)\right) \\
&+ O(\varepsilon^2)
\end{aligned}$$

$$\begin{aligned}
V_1 = &c\boldsymbol{t}_1^{(1)} - W \cdot \boldsymbol{t}_1 \\
= &\left(\frac{c}{\sigma} x_{0,\alpha} + \varepsilon \frac{c}{\sigma^3}\left[z_{0,\alpha}\left(z_{0,\alpha}x_{1,\alpha} - z_{1,\alpha}x_{0,\alpha}\right)\right]\cos(d\beta) + O(\varepsilon^2)\right) - W \cdot \boldsymbol{t}_1 \\
= &\frac{1}{\sigma}\left(c x_{0,\alpha} - W_0^{(1)} x_{0,\alpha} - W_0^{(3)} z_{0,\alpha}\right) \\
&+ \varepsilon\left(-\frac{1}{\sigma}\left(D_{1,1}W_1^{(1)}x_{0,\alpha} + D_{3,3}W_1^{(3)}z_{0,\alpha}\right) - W_{0,y}\frac{1}{\sigma}y_{1,\alpha}\sin(d\beta)\right. \\
&\quad \left. + \frac{1}{\sigma^3}\left(\left(c - W_0^{(1)}\right)\left[z_{0,\alpha}\left(z_{0,\alpha}x_{1,\alpha} - z_{1,\alpha}x_{0,\alpha}\right)\right] - W_0^{(3)}\left[x_{0,\alpha}\left(-z_{0,\alpha}x_{1,\alpha} + x_{0,\alpha}z_{1,\alpha}\right)\right]\right)\cos(d\beta)\right) \\
&+ O(\varepsilon^2)
\end{aligned}$$

$$
\begin{aligned}
V_2 =& c\boldsymbol{t}_2^{(1)} - W \cdot \boldsymbol{t}_2 \\
=& -\varepsilon c d x_1 \sin(d\beta) + O(\varepsilon^2) \\
& - \Big[\Big(W_0^{(1)} + \varepsilon D_{1,1} W_1^{(1)} + O(\varepsilon^2) \Big) \left(-\varepsilon d x_1 \sin(d\beta) + O(\varepsilon^2) \right) \\
& \quad + \left(W_{0,y} + \varepsilon D_{2,2} W_{1,y} + O(\varepsilon^2) \right) \left(1 + O(\varepsilon^2) \right) \\
& \quad + \Big(W_0^{(3)} + \varepsilon D_{3,3} W_1^{(3)} + O(\varepsilon^2) \Big) \left(-\varepsilon d z_1 \sin(d\beta) + O(\varepsilon^2) \right) \Big] \\
=& - W_{0,y} \\
& + \varepsilon \left(d W_0^{(1)} x_1 - W_{1,y} + d W_0^{(3)} z_1 - c d x_1 \right) \sin(d\beta) \\
& + O(\varepsilon^2)
\end{aligned}
$$

Remaining Terms

Note that since $W_{0,y} = 0$, V_2 and μ_β are both only $O(\varepsilon)$, and therefore their product can be neglected in the following terms:

$$
\begin{aligned}
\frac{(\boldsymbol{V} \cdot \nabla)}{\sqrt{E}} \mu =& \frac{1}{\sqrt{E}} \left(V_1 \mu_\alpha + V_2 \mu_\beta \right) = \frac{1}{\sqrt{E}} V_1 \mu_\alpha \\
=& \frac{1}{\sigma^2} \mu_{0,\alpha} \left(c x_{0,\alpha} - W_0^{(1)} x_{0,\alpha} - W_0^{(3)} z_{0,\alpha} \right) \\
& + \varepsilon \Bigg(\frac{1}{\sigma^2} \Big[\mu_{1,\alpha} \left(c x_{0,\alpha} - W_0^{(1)} x_{0,\alpha} - W_0^{(3)} z_{0,\alpha} \right) \\
& \quad - \mu_{0,\alpha} \left(D_{1,1} W_1^{(1)} x_{0,\alpha} + D_{3,3} W_1^{(3)} z_{0,\alpha} \right) \Big] \\
& \quad + \frac{1}{\sigma^4} \mu_{0,\alpha} \Big[\left(c - W_0^{(1)} \right) \left[z_{0,\alpha} \left(z_{0,\alpha} x_{1,\alpha} - z_{1,\alpha} x_{0,\alpha} \right) \right] \\
& \quad - W_0^{(3)} \left[x_{0,\alpha} \left(-z_{0,\alpha} x_{1,\alpha} + x_{0,\alpha} z_{1,\alpha} \right) \right] \\
& \quad - \left(x_{0,\alpha} x_{1,\alpha} + z_{0,\alpha} z_{1,\alpha} \right) \left(c x_{0,\alpha} - W_0^{(1)} x_{0,\alpha} - W_0^{(3)} z_{0,\alpha} \right) \Big] \cos(d\beta)
\end{aligned}
\tag{56}
$$

$$
\begin{aligned}
|W|^2 =& \Big[\Big(W_0^{(1)} + \varepsilon D_{1,1} W_1^{(1)} + O(\varepsilon^2)\Big)\Big(W_0^{(1)} + \varepsilon D_{1,1} W_1^{(1)} + O(\varepsilon^2)\Big) \\
&+ \big(W_{0,y} + \varepsilon D_{2,2} W_{1,y} + O(\varepsilon^2)\big)\big(W_{0,y} + \varepsilon D_{2,2} W_{1,y} + O(\varepsilon^2)\big) \\
&+ \Big(W_0^{(3)} + \varepsilon D_{3,3} W_1^{(3)} + O(\varepsilon^2)\Big)\Big(W_0^{(3)} + \varepsilon D_{3,3} W_1^{(3)} + O(\varepsilon^2)\Big)\Big] \\
=& {W_0^{(1)}}^2 + {W_0^{(3)}}^2 \\
&+ \varepsilon 2\left(W_0^{(1)} W_1^{(1)} + W_0^{(3)} W_1^{(3)}\right)\cos(d\beta) + O(\varepsilon^2)
\end{aligned} \tag{57}
$$

$$
\begin{aligned}
&2W \cdot \boldsymbol{t}_1 V_1 = \\
&\frac{2}{\sigma^2}\left(c x_{0,\alpha} - W_0^{(1)} x_{0,\alpha} - W_0^{(3)} z_{0,\alpha}\right)\left(W_0^{(1)} x_{0,\alpha} + W_0^{(3)} z_{0,\alpha}\right) \\
&+ \varepsilon 2\Bigg(\left(W_0^{(1)} x_{0,\alpha} + W_0^{(3)} z_{0,\alpha}\right)\left(-\frac{1}{\sigma^2}\left(W_1^{(1)} x_{0,\alpha} + W_1^{(3)} z_{0,\alpha}\right)\right. \\
&\left.+\frac{1}{\sigma^4}\left(\left(c - W_0^{(1)}\right)\left[z_{0,\alpha}\left(z_{0,\alpha} x_{1,\alpha} - z_{1,\alpha} x_{0,\alpha}\right)\right] - W_0^{(3)}\left[x_{0,\alpha}\left(-z_{0,\alpha} x_{1,\alpha} + x_{0,\alpha} z_{1,\alpha}\right)\right]\right)\right) + \\
&\quad\left(c x_{0,\alpha} - W_0^{(1)} x_{0,\alpha} - W_0^{(3)} z_{0,\alpha}\right)\left(\frac{1}{\sigma^2}\left(W_1^{(1)} x_{0,\alpha} + W_1^{(3)} z_{0,\alpha}\right)\right. \\
&\quad+ \frac{1}{\sigma^4}\Big(W_0^{(1)}\left[z_{0,\alpha}\left(z_{0,\alpha} x_{1,\alpha} - z_{1,\alpha} x_{0,\alpha}\right)\right] \\
&\quad\left.\left.+ W_0^{(3)}\left[x_{0,\alpha}\left(-z_{0,\alpha} x_{1,\alpha} + x_{0,\alpha} z_{1,\alpha}\right)\right]\Big)\right)\cos(d\beta) + O(\varepsilon^2)
\end{aligned} \tag{58}
$$

$W \cdot \boldsymbol{t}_2, V_2$ and μ_β are all $O(\varepsilon)$, and so $2W \cdot \boldsymbol{t}_2 V_2$ need not be evaluated, and $\frac{1}{4E}\left|\nabla\mu\right|^2$ simplifies to:

$$
\begin{aligned}
\frac{1}{4E}\left|\nabla\mu\right|^2 =& \frac{1}{4E}\left(\mu_\alpha^2 + \mu_\beta^2\right) = \frac{1}{4E}\mu_\alpha^2 \\
=& \left(\frac{1}{4\sigma^2} - \varepsilon\left(\frac{\left(x_{0,\alpha} x_{1,\alpha} + z_{0,\alpha} z_{1,\alpha}\right)}{2\sigma^4}\right)\cos(d\beta) + O(\varepsilon^2)\right) \\
&\left(\mu_{0,\alpha}^2 + \varepsilon 2\mu_{0,\alpha}\mu_{1,\alpha}\cos(d\beta) + O(\varepsilon^2)\right) \\
=& \frac{1}{4\sigma^2}\mu_{0,\alpha}^2 + \varepsilon\left(\frac{1}{2\sigma^4}\left(\sigma^2\mu_{0,\alpha}\mu_{1,\alpha} - \mu_{0,\alpha}^2\left(x_{0,\alpha} x_{1,\alpha} + z_{0,\alpha} z_{1,\alpha}\right)\right)\right)\cos(d\beta) + O(\varepsilon^2)
\end{aligned} \tag{59}
$$

and finally, the gravity term:

$$gz = gz_0 + \varepsilon g z_1 \cos(d\beta) \tag{60}$$

The $O(\varepsilon)$ parts of these separate terms will be combined for the linearization of the Bernoulli equation.

VI. Numerical Simulation of the Vortex Sheet Model

The dimension-breaking procedure was applied to the vortex sheet formulation with reduced small-scale approximation for several different parameter sets. As a demonstration of the results, the bulk of the figures and data presented here are for $\tau = 0, g = 1, \mathrm{At} = 0.1$ and are specified as such. Several figures are presented and identified with different parameters to show that the procedure was not limited to one particular parameter set.

To begin, bifurcation periods were calculated for waves of increasing height and are graphed in Figure 15. Additionally, a log-log plot of the periods against wave height is presented in Figure 16. Note that the reference line is $O(1/h)$. For this particular model the wave began to form cusps and the solver no longer converged to a solution beyond the maximum height plotted, but there is an observable deviation from the small amplitude asymptotic at the larger wave heights.

The bifurcation periods have dependence on planar wave height, Atwood number, surface tension and gravity. Figure 17 shows the bifurcation periods as a surface with height and Atwood number fixed, gravity ranging from 0.1 to 1 and surface tension from 0.1 to 2. It is notably smooth suggesting continuous dependence on these last two parameters, with a significant decrease as $g \to 0$.

In addition to the bifurcation period, $Ly = 1/d$, perturbation functions of α are calculated using the linearization and dimension-breaking procedure. Figure 18 shows an example set of four perturbation functions, x_1, y_1, z_1, μ_1, for the bifurcation at speed $c = 0.307$ with parameters $\tau = 0, g = 1, \mathrm{At} = 0.1$. In Figure 19, we compare the actual variation from the planar wave as found by the solver against the ansatz for this bifurcation. This is done by taking the infinity-norm of the difference of the two functions. The difference between all calculated perturbation functions and the solved values are trending down on the order of ε^2, indicating that the linearization

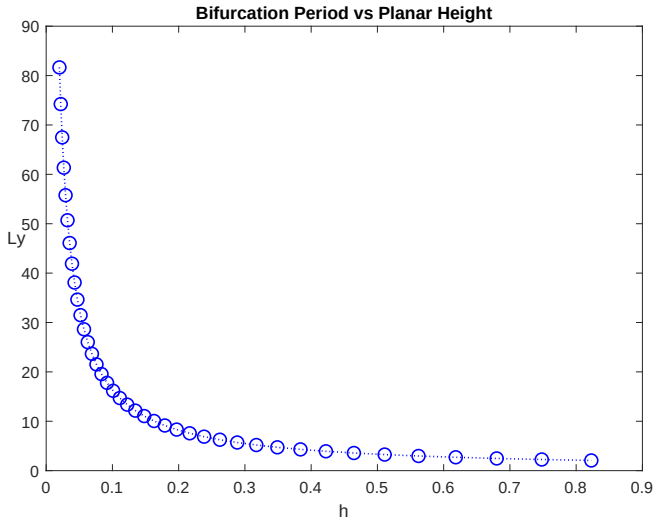

Figure 15. Bifurcation period, $Ly = 2\pi/d$ as a function of planar wave height, $h = \max(z) - \min(z)$, for the reduced Small-Scale approximation Vortex Sheet model with parameters $\tau = 0, g = 1,$ At $= 0.1$.

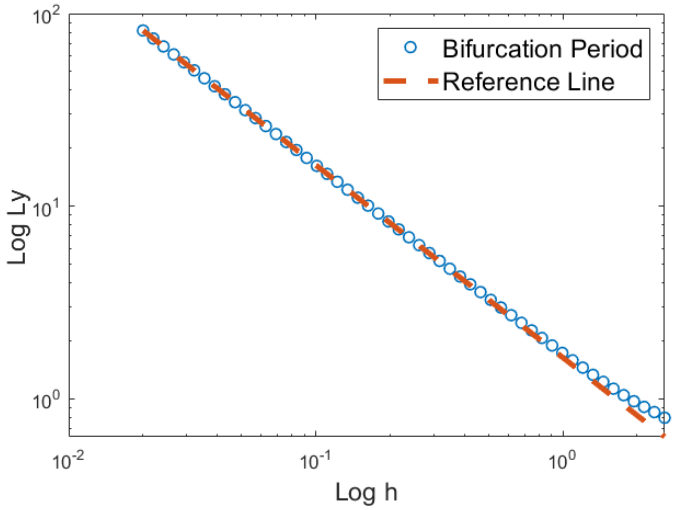

Figure 16. Log-Log plot of bifurcation periods, $Ly = 2\pi/d$, plotted against height $h = \max(z) - \min(z)$, blue circles, for the reduced Small-Scale approximation Vortex Sheet model with parameters $\tau = 0, g = 1,$ At $= 0.1$. The same behavior was observed with parameters $\tau = 2, g = 0,$ At $= 1$. The reference line, red dashed line, is $O(1/h)$ is to compare the deviation away from the small-amplitude asymptotic.

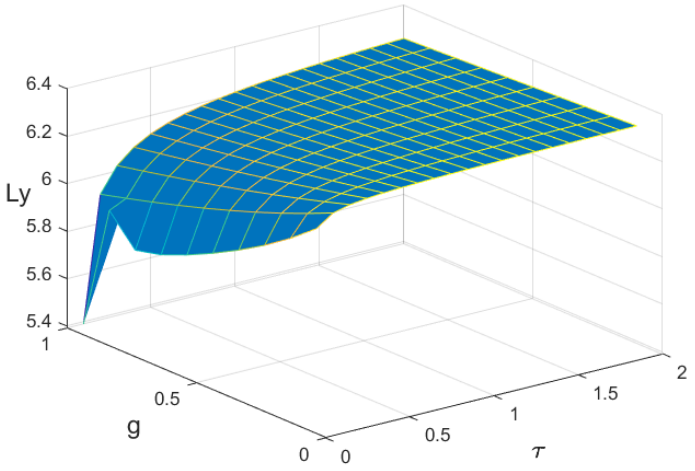

Figure 17. Bifurcation periods, $Ly = 2\pi/d$, of the vortex sheet model plotted against gravity, g, and surface tension, τ. All iterations were with an Atwood number of 0.5 and bifurcated from a planar wave of height $h = 0.0505$

ansatz is valid.

Using the calculated search direction, comprised of the bifurcation period and perturbation functions, a variety of fully-three-dimensional waves were computed. These waves were tested with parameters $\tau = 0, g = 1, \mathrm{At} = 0.1$ to bifurcate from planar waves of speed $c = 0.316, 0.3148, 0.3131,$ and 0.307. These tests demonstrated that the procedure yields valid solutions at many wave speeds, however as the results are all similar, they are not all presented.

The Speed/Amplitude plot in Figure 20 for the reduced small-scale approximation model shows the planar wave branch as the dashed red line. It is zoomed in to emphasize the accuracy of several of the bifurcations, blue diamonds, derived from the dimension-breaking procedure.

Additional Speed/Amplitude plots are presented in Figures 21, 22, and 23 for different parameter sets. The parameters are identified in each figure caption and all follow the same labeling conventions of Figure 20.

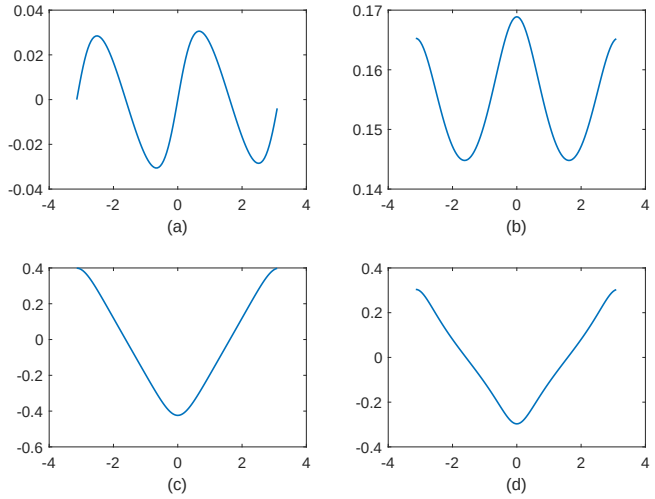

Figure 18. Example Perturbation functions (a) x_1, (b) y_1, (c) z_1, and (d) μ_1 for the two-dimensional wave at speed $c = 0.307$.

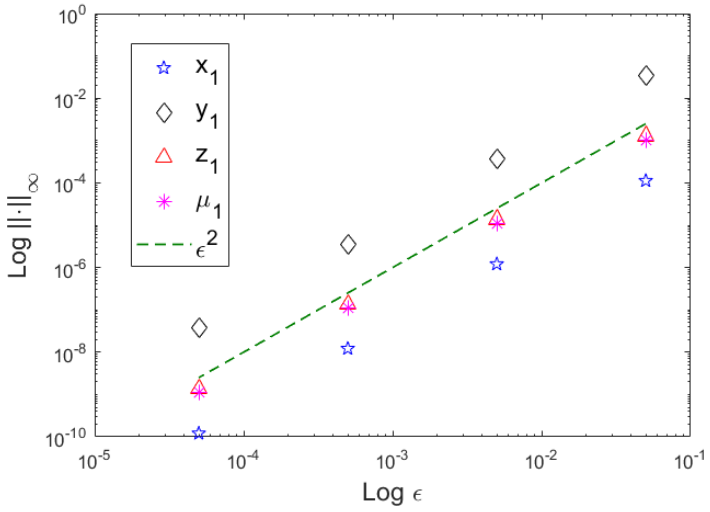

Figure 19. The norm between the calculated perturbation functions from the dimension-breaking continuation procedure and the actual waves computed in the full solver are compared against ε^2, dashed green line, for reference in a log-log plot. The symbols are labeled in the legend as to which perturbation function they represent.

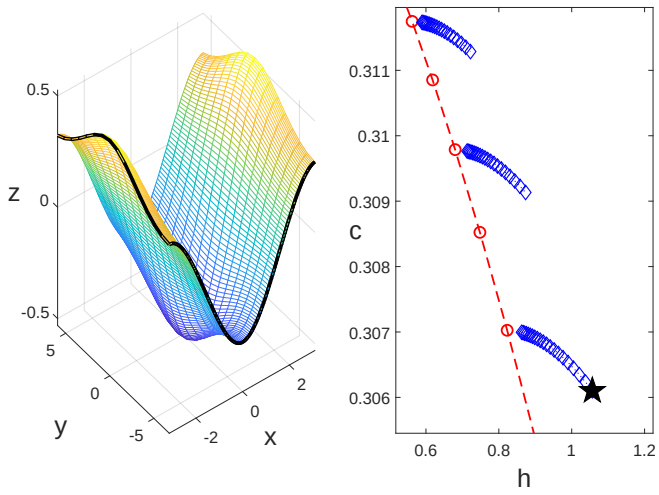

Figure 20. Speed/Amplitude plot of reduced small-scale approximation in the vortex sheet formulation with $\tau = 0, g = 1, At = 0.1$. Planar waves are shown as the dashed red line. c is wave speed and the amplitude $h = \max(z) - \min(z)$. Several bifurcations are shown occurring at multiple starting speeds and continuing in the fully three-dimensional vortex sheet model, Equations (24)-(27), blue diamonds. The wave at left bifurcated from speed $c = 0.307$ and is marked on the plot with the large black star.

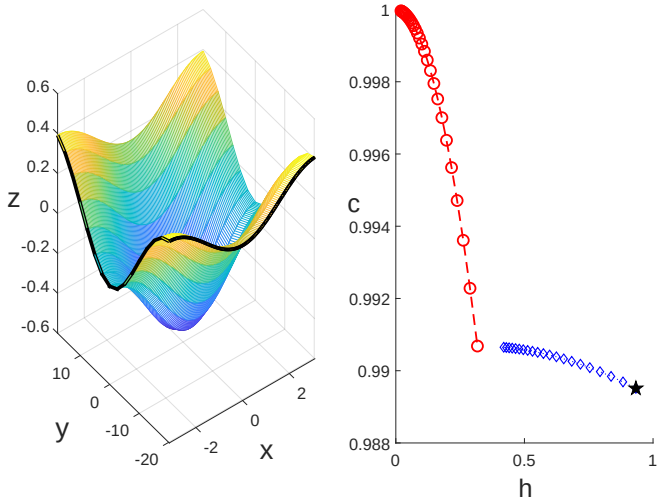

Figure 21. Speed/Amplitude plot of reduced small-scale approximation in the vortex sheet formulation with $\tau = 1, g = 0, At = 1$.

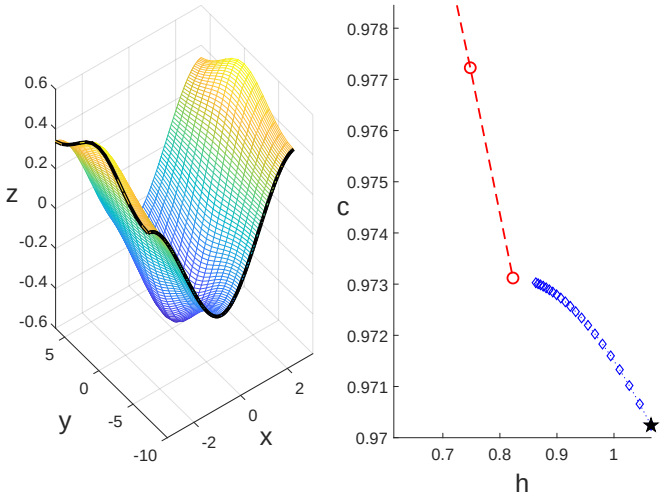

Figure 22. Speed/Amplitude plot of reduced small-scale approximation in the vortex sheet formulation with $\tau = 0, g = 2, At = 0.5$.

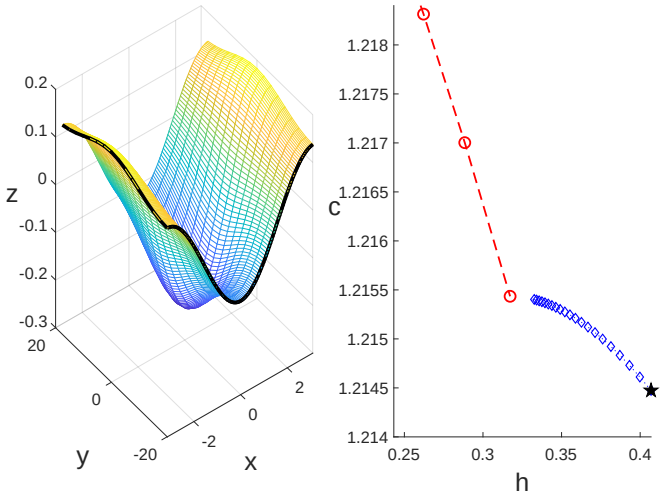

Figure 23. Speed/Amplitude plot of reduced small-scale approximation in the vortex sheet formulation with $\tau = 2, g = 0.5, At = 1$.

VII. Conclusion

Overall, this study has shown the proposed dimension-breaking continuation procedure to be effective at generating search directions for an (N+1)-dimensional solver. The procedure has been applied to both single evolution equations and a system of equations. Computational results of bifurcations from KdV to KP solutions were compared to the previous work of Groves, Haragus and Sun [4] and shown to be in agreement with their explicit formulas.

The bifurcations from the Akers-Milewski model are new results that show this work to be a valid concept. The small-amplitude asymptotics agree with similar wave packets from Milewski and Wang [39]. This procedure is also able to generate bifurcation parameters beyond where it is in agreement with the asymptotics.

Applied to the vortex sheet formulation, this work was able to account for the d dependency of the pseudo-differential operators in the linearization. The $W^{(2)}$ and $W^{(3)}$ terms of the Birkhoff-Rott integral in the reduced model of Section 4.4 contains all of the complexity found in the small-scale version.

While overturning waves have not yet been achieved with the dimension-breaking continuation procedure, all of the difficulties leading up to the small-scale approximation model have been handled and produced accurate results. This suggests that the dimension-breaking continuation procedure will be able to generate accurate search directions in the small-scale approximation, facilitating the work of the solver with a valid initial guess and thereby eliminating the need to repeatedly guess-and-check.

7.1 Future Work

The next step in this work is to re-introduce the $W^{(1)}$ term to the vortex sheet model (24) - (27) with small-scale approximation, equation (37). The vortex sheet

model with small-scale approximation supports overturned traveling waves and will directly contribute in line with the work of Akers and Reeger [26]. After achieving this, we will move to linearize the full Birkhoff-Rott integral. This procedure should also be applied to other weakly-nonlinear models such as other variations stemming from the work of Akers and Milewski [49, 50, 21] and in the Ablowitz-Fokas-Musslimani model [34].

Finally, note that while the dimension-breaking continuation procedure is applied to traveling water waves in this study, it is not limited to them. The ideas of this thesis generalize to PDEs arising in other areas, for example in lasers and weather phenomena. The general dimension-breaking continuation procedure outlined in Section 2.1 can be used on an equilibria state in any model to bifurcate to the next higher dimension from the lower dimension.

Bibliography

1. P. A. Milewski, J.-M. Vanden-Broeck, and Z. Wang, "Dynamics of steep two-dimensional gravity-capillary solitary waves," *Journal of Fluid Mechanics*, vol. 664, pp. 466–477, 2010.

2. Z. Wang and P. A. Milewski, "Dynamics of gravity-capillary solitary waves in deep water," *Journal of Fluid Mechanics*, vol. 708, pp. 480–501, 2012.

3. D. P. Nicholls and F. Reitich, "Stable, high-order computation of traveling water waves in three dimensions," *European Journal of Mechanics, B/Fluids*, vol. 25, no. 4, pp. 406–424, 2006.

4. M. Groves, M. Haragus, and S. Sun, "A dimension-breaking phenomenon in the theory of steady gravity-capillary water waves," *Philosophical Transactions of the Royal Society A: Mathematical, Physical and Engineering Sciences*, vol. 360, no. 1799, 2002.

5. D. J. Emmons, D. E. Weeks, B. Eshel, and G. P. Perram, "Metastable Ar (1s5) density dependence on pressure and argon-helium mixture in a high pressure radio frequency dielectric barrier discharge," *Journal of Applied Physics*, vol. 123, no. 4, 2018.

6. R. Rezaei, P. Eckert, J. Seebode, and K. Behnk, "Zero-Dimensional Modeling of Combustion and Heat Release Rate in DI Diesel Engines," *SAE International Journal of Engines*, vol. 5, no. 3, pp. 874–885, 2012.

7. J. S. Russell, *Report on Waves*. London: Richard and John Taylor, 1845.

8. A. D. Craik, "the Origins of Water Wave Theory," *Annual Review of Fluid Mechanics*, vol. 36, no. 1, pp. 1–28, 2004.

9. G. G. Stokes, "On the Theory of Oscillitory Waves," in *Mathematical and Physical Papers*, p. 328, Cambridge University Press, 1880.

10. A. D. Craik, "George Gabriel Stokes on Water Wave Theory," *Annual Review of Fluid Mechanics*, vol. 37, no. 1, pp. 23–42, 2005.

11. D. J. Korteweg and G. de Vries, "XLI. On the change of form of long waves advancing in a rectangular canal, and on a new type of long stationary waves," *Philosophical Magazine Series 5*, vol. 39, no. 240, pp. 422–443, 1895.

12. G. D. Crapper, "An exact solution for progressive capillary waves of arbitrary amplitude," *Journal of Fluid Mechanics*, vol. 2, no. 6, pp. 532–540, 1957.

13. M. Haragus and K. Kirchgässner, "Breaking the Dimension of a Steady Wave: Some Examples," in *Nonlinear Dynamics and Pattern Formation in the Natural Environment* (A. Doelman and A. van Harten, eds.), pp. 119–129, 1995.

14. B. B. Kadomtsev and V. I. Petviashvili, "On the Stability of Solitary Waves in Weakly Dispering Media," *Doklady Akademii Nauk SSSR*, vol. 192, no. 4, pp. 753–756, 1970.

15. M. Tajiri and Y. Murakami, "The periodic solution resonance: solutions of the Kadomtsev-Petviashvili equation with positive dispersion," *Physics Letters A*, vol. 143, pp. 217–220, 1990.

16. L. Deike, W. Mostert, W. Melville, and S. Popinet, "Direct numerical simulations of breaking wave in deep and shallow water," 2018.

17. M. Conrath, P. J. Canfield, P. M. Bronowicki, M. E. Dreyer, M. M. Weislogel, and A. Grah, "Capillary Channel Flow Experiments Aboard the International Space Station," *Physical Review E*, vol. 88, p. 063009, 2013.

18. D. I. Meiron and P. G. Saffman, "Overhanging interfacial gravity waves of large amplitude," *Journal of Fluid Mechanics*, vol. 129, pp. 213–218, 1983.

19. H. Okamoto and M. Shõji, *The Mathematical Theory of Permanent Progressive Water-Waves*, vol. 20 of *Advanced Series in Nonlinear Dynamics*. WORLD SCIENTIFIC, sep 2001.

20. J.-M. Vanden-Broeck, *GravityCapillary Free-Surface Flows*. Cambridge: Cambridge University Press, 2010.

21. B. F. Akers and D. P. Nicholls, "Traveling Water Waves with Gravity and Surface Tension," *SIAM Journal of Applied Mathematics*, vol. 70, pp. 2373–2389, 2010.

22. O. Trichtchenko, B. Deconinck, and J. Wilkening, "The instability of Wilton ripples," *Wave Motion*, vol. 66, pp. 147–155, 2016.

23. B. F. Akers, D. M. Ambrose, and J. D. Wright, "Gravity perturbed Crapper waves," *Proceedings of the Royal Society A: Mathematical, Physical and Engineering Sciences*, vol. 470, no. 2161, 2013.

24. B. F. Akers, D. M. Ambrose, K. Pond, and J. D. Wright, "Overturned internal capillary-gravity waves," *European Journal of Mechanics, B/Fluids*, vol. 57, pp. 143–151, 2016.

25. B. F. Akers, D. M. Ambrose, and J. D. Wright, "Traveling waves from the arclength parameterization: Vortex sheets with surface tension," *Interfaces and Free Boundaries*, vol. 15, no. 3, pp. 359–380, 2013.

26. B. F. Akers and J. A. Reeger, "Three-dimensional overturned traveling water waves," *Wave Motion*, vol. 68, pp. 210–217, 2017.

27. S. H. Lamb, *Hydrodynamics*. 1932.

28. D. J. Acheson, *Elementary fluid dynamics*. Clarendon Press, 1990.

29. D. M. Ambrose, W. A. Strauss, and J. D. Wright, "Global bifurcation theory for periodic traveling interfacial gravitycapillary waves," *Annales de l'Institut Henri Poincare (C) Analyse Non Lineaire*, vol. 33, no. 4, pp. 1081–1101, 2016.

30. D. P. Nicholls and J. Shen, "A rigorous numerical analysis of the transformed field expansion method," *SIAM Journal of Numerical Analysis*, vol. 47, no. 4, pp. 2708–2734, 2009.

31. V. E. Zakharov, "Stability of periodic waves of finite amplitude on the surface of a deep fluid," *Journal of Applied Mechanics and Technical Physics*, vol. 9, pp. 190–194, 1968.

32. W. Craig and C. Sulem, "Numerical Simulation of Gravity Waves," *Journal of Computational Physics*, vol. 108, pp. 73–83, 1993.

33. J. Wilkening and V. Vasan, "Comparison of Five Methods of Computing the DirichletNeumann Operator for the Water Wave Problem," in *Contemporary Mathematics*, pp. 175–210, 2013.

34. M. J. Ablowitz, A. S. Fokas, and Z. H. Musslimani, *On a new non-local formulation of water waves*, vol. 562. 2006.

35. K. Oliveras and V. Vasan, "A new equation describing travelling water waves," *Journal of Fluid Mechanics*, 2013.

36. H. Poincaré, "Sur l'équilibre d'une masse fluide animée d'un mouvement de rotation," *Acta Mathematica*, 1885.

37. B. F. Akers and P. A. Milewski, "Dynamics of Three-dimensional Gravity-capillary Solitary Waves in Deep Water," *J. APPL. MATH.*, vol. 70, pp. 2390–2408, jan 2010.

38. J. D. DIORIO, Y. CHO, J. H. DUNCAN, and T. R. AKYLAS, "Resonantly forced gravitycapillary lumps on deep water. Part 1. Experiments," *Journal of Fluid Mechanics*, 2011.

39. P. A. Milewski and Z. Wang, "Transversally periodic solitary gravity-capillary waves," *Proceedings of the Royal Society A: Mathematical, Physical and Engineering Sciences*, vol. 470, no. 2161, pp. 20130537–20130537, 2013.

40. S. Alben, "Flag flutter in inviscid channel flow," *Physics of Fluids*, 2015.

41. D. M. Ambrose and M. Siegel, "A non-stiff boundary integral method for 3D porous media flow with surface tension," in *Mathematics and Computers in Simulation*, 2012.

42. D. M. Ambrose, M. Siegel, and S. Tlupova, "A small-scale decomposition for 3D boundary integral computations with surface tension," *Journal of Computational Physics*, vol. 247, pp. 168–191, 2013.

43. P. G. Saffman, *Vortex Dynamics*. Cambridge: Cambridge University Press, 1992.

44. R. E. Caflisch and X. F. Li, "Lagrangian Theory for 3D Vortex Sheets with Axial or Helical Symmetry," *Transport Theory and Statistical Physics*, 1992.

45. D. M. Ambrose and N. Masmoudi, "The zero surface tension limit two-dimensional water waves," *Communications on Pure and Applied Mathematics*, vol. 58, no. 10, pp. 1287–1315, 2005.

46. M. J. Ablowitz and A. S. Fokas, *Complex Variables: Introduction and Applications*. Cambridge: Cambridge University Press, 2nd ed., 2003.

47. T. Y. Hou, G. Hu, and P. Zhang, "Singularity formation in three-dimensional vortex sheets," *Physics of Fluids*, 2003.

48. L. N. L. N. Trefethen and D. Bau, *Numerical linear algebra*. Society for Industrial and Applied Mathematics, 1997.

49. B. F. Akers and P. A. Milewski, "Model equations for gravity-capillary waves in deep water," *Studies in Applied Mathematics*, vol. 121, no. 1, pp. 49–69, 2008.

50. B. F. Akers and P. A. Milewski, "A model equation for wavepacket solitary waves arising from capillary-gravity flows," *Studies in Applied Mathematics*, vol. 122, no. 3, pp. 249–274, 2009.

REPORT DOCUMENTATION PAGE

Form Approved
OMB No. 0704-0188

1. REPORT DATE *(DD-MM-YYYY)*	**2. REPORT TYPE**	**3. DATES COVERED** *(From - To)*
09-2-2019	Doctoral Dissertation	Sept 2017-Aug 2019

4. TITLE AND SUBTITLE

DIMENSION-BREAKING FOR TRAVELING WAVES IN INTERFACIAL FLOWS

5a. CONTRACT NUMBER

5b. GRANT NUMBER

5c. PROGRAM ELEMENT NUMBER

6. AUTHOR(S)

Seiders, Matthew W., Maj.

5d. PROJECT NUMBER

5e. TASK NUMBER

5f. WORK UNIT NUMBER

7. PERFORMING ORGANIZATION NAME(S) AND ADDRESS(ES)

Air Force Institute of Technology
Graduate School of Engineering and
Management (AFIT/EN)
2950 Hobson Way
WPAFB, OH 45433

8. PERFORMING ORGANIZATION REPORT NUMBER

AFIT-EN-DS-19-S-002

9. SPONSORING / MONITORING AGENCY NAME(S) AND ADDRESS(ES)

Intentionally left blank.

10. SPONSOR/MONITOR'S ACRONYM(S)

11. SPONSOR/MONITOR'S REPORT NUMBER(S)

12. DISTRIBUTION / AVAILABILITY STATEMENT

Distribution Statement A. Approved for Public Release; Distribution Unlimited

13. SUPPLEMENTARY NOTES

14. ABSTRACT

Fluid flow models in two spatial dimensions with a one-dimensional interface are known to support overturned traveling solutions. Computational methods of solving the two-dimensional problem are well developed, even in the case of overturned waves. The three-dimensional problem is harder for three prominent reasons. First, some formulations of the two-dimensional problem do not extend to three-dimensions. The technique of conformal mapping is a prime example, as it is very efficient in two dimensions but does not have a three-dimensional equivalent. Second, some three-dimensional models, such as the Transformed Field Expansion method, do not allow for overturned waves. Third, computational time can increase by more than an order of magnitude. For example, the Birkhoff-Rott integral has a cost of O(N^2) in two-dimensions but O(N^4M^2) in three-dimensions, where N is the number of discretized points in the lateral directions and M is the number of truncated summation terms.

This study seeks to bridge the gap between efficient two-dimensional numerical solvers and more computationally expensive three-dimensional solvers. The dissertation does so by developing a dimension-breaking continuation method, which is not limited to solving interfacial wave models. The method involves three steps: first, conduct N-dimensional continuation to large amplitude; second, extend the solution trivially to a (N+1)-dimensional solution and solve the linearization; and third, use the linearization to begin (N+1)-dimensional continuation. This method is successfully applied to Kadomtsev-Petviashvili and Akers-Milewski interfacial models and then in a reduced Vortex Sheet interfacial formulation. In doing so, accurate search directions are calculated for use in higher-dimension quasi-Newton solvers.

15. SUBJECT TERMS

16. SECURITY CLASSIFICATION OF:			**17. LIMITATION OF ABSTRACT**	**18. NUMBER OF PAGES**	**19a. NAME OF RESPONSIBLE PERSON**
a. REPORT	**b. ABSTRACT**	**c. THIS PAGE**			Dr. Benjamin Akers, AFIT/ENC
U	U	U	U	82	**19b. TELEPHONE NUMBER** (937) 255-3636x4522, benjamin.akers@afit.edu